

Algorithms for Gibbs state preparation on noiseless and noisy random quantum circuits

Oles Shtanko^{1,*} and Ramis Movassagh^{2,†}

¹*IBM Quantum, IBM Research, Almaden, San Jose CA, 95120, USA*

²*IBM Quantum, MIT-IBM Watson AI lab, Cambridge MA, 02142, USA*

The most promising and practical candidate to demonstrate a drastic advantage of quantum computers over classical ones is the simulation of quantum matter. Despite the advances in simulation of the time evolution, preparing thermal states of quantum many-body systems remains notoriously a difficult yet important task. The existing algorithms either require quantum phase estimation [1–4] rendering them impractical for current noisy hardware, or are variational [5–7] which face obstacles such as initialization, barren plateaus, and a general lack of provable convergence. We propose two quantum algorithms with provable guarantees to prepare thermal states on current noisy quantum hardware. The first algorithm requires postselection on intermediate measurements and runs on a quantum circuit with $\text{poly}(n)$ depth, where n is the number of qubits. This algorithm requires a significantly smaller number of gates than previous such algorithms. The second algorithm is tailored to ergodic interacting systems which are a vast subset of physical Hamiltonians. This algorithm can potentially sample thermal distributions in polynomial time. In addition, both of our algorithms have free parameters that can be optimized or trained to mitigate noise and computational errors. We illustrate our algorithms by running them on the latest IBM quantum hardware and in particular simulate them for the Fermi-Hubbard model.

Quantum computers promise to drastically outperform traditional computers. Perhaps the most striking practical candidate to demonstrate this advantage is to simulate quantum matter, which was Feynman’s original motivation for proposing the quantum computers. The equilibrium thermal Gibbs state is the most prevalent macrostate of quantum matter. Thermal states are therefore essential for the study of many-body systems; applications include quantum chemistry and materials science [8, 9], high-energy physics [10], and computer science [11]. Classical computers are ineffective in simulating quantum many-body states due to the sign problem that requires resources exponential in the system size [12]. The classical computers’ computational predicament is especially pronounced for strongly interacting quantum matter which underpins the richness of quantum phenomena such as quantum phase transitions. Quantum computers, however, have the power to simulate quantum processes such as thermal equilibration [13], which suggests that quantum computing might be efficient for simulating the thermodynamic properties. Despite the well-developed quantum algorithms for the time evolution [14], preparing thermal or ground states of interacting quantum matter is far less developed.

Quantum algorithms for thermal state preparation have a long history, partially summarized in Ref. [8]. Earlier work provided an empirical algorithm using the idea of emulating a generic “digital bath” consisting of ancilla qubits [15]. Later works utilize exact algorithms using quantum phase estimation that allows performing computation in the eigenbasis of the Hamiltonian [1, 2]. A remarkable example of such a method is the quantum

Metropolis algorithm [3, 4, 16] which is a technique for directly sampling the eigenstates of the Hamiltonian with Gibbs probabilities. While several methods were proposed for reducing the required computational resources [17, 18], they need the quantum phase-estimation subroutine, whose experimental realization has proven to be difficult on near-term noisy quantum computers which do not have fault-tolerance. In order to circumvent this problem, variational hybrid quantum-classical algorithms were proposed for reducing the circuit depth and consequently the aggregated error [5–7]. However, variational algorithms do not provide a provable advantage over classical computers nor can they output be certified to be close to the thermal state [19]. Recently, a different quantum-classical algorithm for imaginary-time evolution was proposed [20, 21]; whose accuracy beyond short-range correlated systems remains unknown and its performance takes exponential time. In parallel there has been a surge of activity to do thermal state preparation in driven-dissipative quantum systems [22–25], which can be compared to the existing methods of algorithmic cooling [26–28]. However, the fidelity of dissipative thermal state preparation remains low due to a lack of sufficient control.

In this paper, we propose two new algorithms for preparing thermal states that require smaller computational resources than the previous works. These algorithms have the further amenity that they have adjustable parameters to mitigate noise. The proposed algorithms are thus suitable for the near-term quantum computers and can potentially overcome the drawbacks in the aforementioned various different techniques for thermal state preparation. Additionally, the circuit implementing the algorithms have the same locality as the underlying Hamiltonian.

In Algorithm 1, we utilize random quantum circuits

* oles.shtanko@ibm.com

† ramis@us.ibm.com

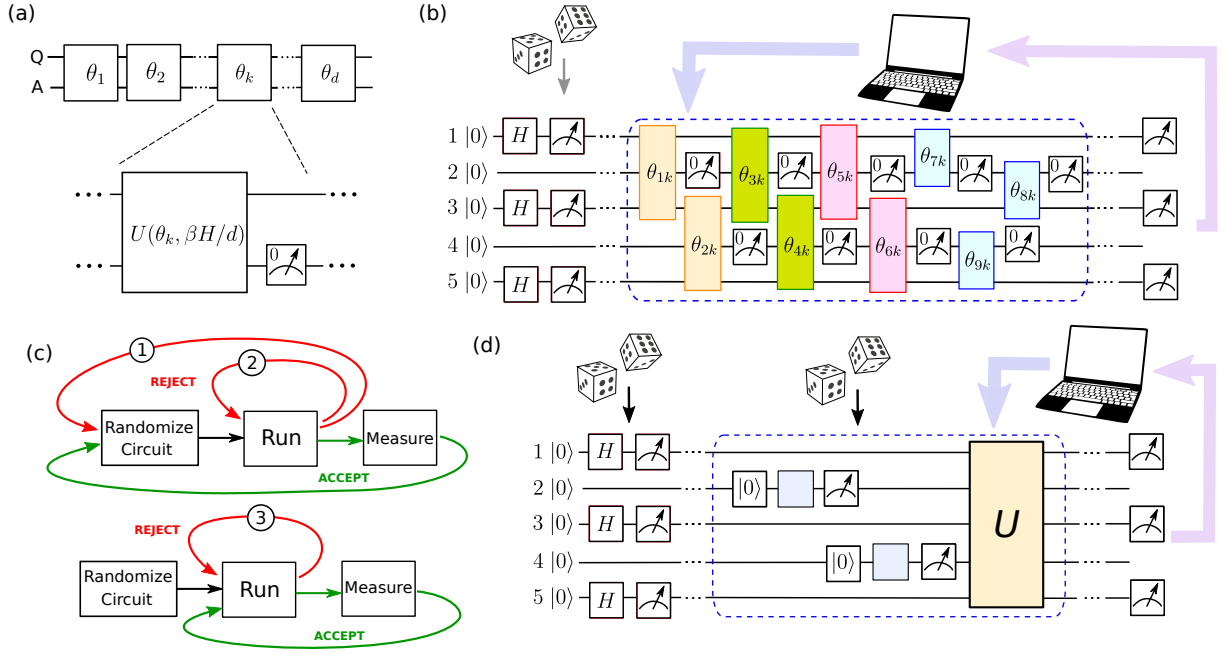


FIG. 1. **Algorithms implementation.** (a) Circuit implementing imaginary-time evolution using Algorithm 1 by d random unitary gates (see Eq. (2)) with following ancilla measurements and postselection (denoted by label “0” inside the measurement element). (b) Application for the Hamiltonian in Eq. (15) for $n = 3$ system qubits and $n_a = 2$ ancilla qubits. Qubits 1, 3, 5 serve as the system qubits and 2, 4 are ancilla qubits. Orange gate color (θ_{1k}, θ_{2k}) is for the XX -terms in the Hamiltonian, green (θ_{3k}, θ_{4k}) is for YY -terms, pink (θ_{5k}, θ_{6k}) are for ZZ -terms, and blue (θ_{7k}, θ_{8k} and θ_{9k}) are for Z -terms. In the noise-mitigation mode, classical computer estimates the cost function (e.g., free energy) and adjusts the circuit to reduce the error. (c) Different modes of Algorithm 1. The top panel shows the modes 1 and 2 where the circuit is randomized after sample measurements. For mode 1, the circuit angles Θ are being reset after each run, while for mode 2 it happens only after accepted run. The bottom panel shows the mode 3, where the circuit is fixed for the entire computation process. (d) Schematics for Algorithm 2 utilizing $n = 3$ system qubits and $n_a = 2$ ancilla qubits. As for panel (a), the system qubits are first initialized in a random product state. Next, the ancilla is reset at each cycle in the individual thermal states using single-qubit gate and a measurement, and a unitary evolution is implemented under a local Hamiltonian in Eq. (10).

(RQC) with intermediate measurements to sample from the thermal distribution. Furthermore, we show that initially random parameters can be optimized to compensate for the errors, which are primarily induced by limited depth and noise. RQC are known to be analytically feasible and yet comprehensive model of complex quantum dynamics that, for example, exhibits quantum chaos [29] and provide a window for probing quantum phases of matter [30]. Also, RQC have been the workhorse of modern quantum complexity theory as the hardness of sampling their outputs is believed to be the foremost candidate for demonstrating quantum supremacy [31–33]. Nevertheless RQC seemed to have no practical computational utility beyond demonstrating quantum supremacy. Algorithm 1 therefore provides a practical use for RQC in preparing thermal Gibbs states on near-term quantum computers for general Hamiltonian. Despite having relatively small number of gates, Algorithm 1 requires postselection and in agreement with complexity theoretical limitations takes exponential time to run [34–38].

The exponential run-time can be circumvented by Algorithm 2 which works on a sub-class of ergodic Hamiltonians. This algorithm is a development of digital bath

idea [24, 39] with provable efficient performance for the class of Hamiltonians satisfying Eigenstate Thermalization Hypothesis (ETH) [40–44]. A simple corollary of ETH is that the expectation values of local observables with respect to a long-time evolved generic initial state coincide with the Gibbs expectation values. Although ETH is not easily proved for a given Hamiltonian, its universality across various non-integrable quantum many-body systems has been thoroughly studied numerically [45]. Assuming ETH, the run-time of our algorithm is as efficient as the (quantum) Metropolis algorithm [46], which is perhaps the best known empirical algorithm for evaluating thermal expectation values. By adjusting the parameters of both algorithms, we also achieve drastic error reduction in the presence of noise. Algorithm 2 however is simple and, unlike the quantum Metropolis algorithm, does not require the quantum phase estimation subroutine to be performed at every step of the algorithm.

These algorithms have the advantage of combining the positive features of the previously known methods. For example, they have provable convergence to the thermal state, do not require quantum phase estimation

subroutine, and can be optimized and adjusted to noise. Moreover, their optimization-based version, unlike comparable variational methods, may avoid the barren plateau problem [19] as they approach the global minimum for average choice of parameter. These aggregate set of properties make these algorithms particularly suitable for noisy near-term quantum computers.

Algorithm 1. The goal is to obtain samples from the thermal Gibbs distribution

$$\rho_\beta = \mathcal{Z}_\beta^{-1} \exp(-\beta H), \quad (1)$$

where $\mathcal{Z}_\beta = \text{Tr} \exp(-\beta H)$ is the partition function. Algorithm 1 accomplishes this by sampling from the distribution of RQC with $\text{poly}(n)$ depth and intermediate measurements, where n is the number of qubits.

The purpose of randomness is to implement effective imaginary-time evolution (ITE). Starting from a random initial state, ITE produces Gibbs state because $\mathbb{E}_\psi e^{-\beta H/2} |\psi\rangle \langle \psi| e^{-\beta H/2} \propto \exp(-\beta H)$, where ψ is the initial state and \mathbb{E}_ψ denotes the average with respect to a uniform choice over any complete set of basis states (including product states). With no loss of generality, we shift the energy and take the Hamiltonian a positive operator $H \geq 0$. Then, we generate ITE using an average over a family of random unitary operations, $\mathbb{E}_\theta \exp(i\theta\sqrt{2\beta H}) = \exp(-\beta H)$, where $\theta \in \mathcal{N}(0, 1)$ is Gaussian random variable. To implement the average unitary, we construct a dynamical map that utilizes ancilla and measurements [18, 47].

We then define each of the d layers of the quantum circuit by the following $(n+1)$ -qubit unitary operator

$$U(\theta_k, \beta H/d) := \exp\left(i\theta_k \sqrt{\beta H/d} \otimes X\right), \quad (2)$$

where $\theta_k \in \mathcal{N}(0, 1)$ are independently chosen for each $k \in \{1, 2, \dots, d\}$, the Pauli operator X acts on the ancilla qubit, and the Hamiltonian H acts on the remaining n system qubits. After each layer, we measure the ancilla qubit, reset it, and accept if the measurement returns zero (see Fig. 1(a)). If accepted, we proceed to the next layer. Otherwise we re-run the circuit after resetting the values of θ_k . The resulting distribution is described by a circuit-averaged density matrix

$$\tilde{\rho}_{\beta,d} = \mathbb{E}[P_{\beta,d} \rho_{\beta,d}] / \mathbb{E}[P_{\beta,d}], \quad (3)$$

where $\rho_{\beta,d}$ is the successfully accepted final output state and $P_{\beta,d}$ is probability of accepting the circuit, and the expectation is taken with respect to the random angles θ_k .

Starting from a random initial state on the n -qubits (as defined above) and the 1-qubit ancillas initialized to $|0\rangle$, the expected density matrix $\tilde{\rho}_{\beta,d}$ of the n -qubit system after d layers is

$$\tilde{\rho}_{\beta,d} = \frac{1}{2^d \mathcal{Z}_{\beta,d}} \sum_{k=0}^d \binom{d}{k} \exp(-\beta_k H), \quad (4)$$

where $\beta_k = 2\beta k/d$ is discrete inverse temperature, and $\mathcal{Z}_{\beta,d} = \text{Tr}[e^{-\beta H} \cosh^d(\beta H/d)]$ is a modified partition function. In the limit $d \rightarrow \infty$, the binomial distribution asymptotically approaches the delta function with the center at β . Thus, the output converges the desired Gibbs distribution ρ_β as (see Section IB of Supplement)

$$S(\rho_\beta \| \tilde{\rho}_{\beta,d}) \leq O(\beta^4 \text{Var}_\beta(H^2)/d^2), \quad (5)$$

where $S(\sigma \| \rho)$ is the relative entropy, $\text{Var}_\beta(x) := \langle x^2 \rangle_\beta - \langle x \rangle_\beta^2$ is the variance and the expectation is taken with respect to the thermal state, $\langle x \rangle_\beta := \text{Tr}[x \rho_\beta]$. For physical many-body Hamiltonians, the variance $\text{Var}_\beta(H^2) \sim O(n^2)$. Therefore, in order to achieve $S(\sigma \| \rho) \leq \epsilon$ for a fixed error $\epsilon > 0$, the minimal required (non-local) circuit depth is $d \sim O(n\beta^2/\sqrt{\epsilon})$. The run-time of the algorithm grows exponentially with the system size because whenever ancilla results in $|1\rangle$ we re-run the circuit. In general, the acceptance probability for a circuit is $\mathbb{E}[P_{\beta,d}] \geq 2^{-\alpha n}$, where $\alpha = 1 - (\log_2 \mathcal{Z}_\beta)/n \geq 0$ (see Section 1C of Supplement). This conclusion agrees with the fact that the exact preparation of a thermal state for a many-body system is quantum Merlin Arthur (QMA)-complete in general [34–38].

Constructing the square root of a many-body Hamiltonian can be computationally costly. We improve the algorithm, by taking the system Hamiltonian to be of the form $H = \sum_{m=1}^M h_m$, where $h_m \geq 0$ are positive local terms (each acting on a constant number of qubits) with the total number of local terms being M . Then, we obtain the corresponding product of M local unitary gates replace the single operation in Eq. (2), akin to the Suzuki-Trotter method [14, 48]. Each gate has the form $U(\theta_{mk}, \beta h_m/d)$, $\theta_{mk} \in \mathcal{N}(0, 1)$, followed by ancilla measurement and post-selection to zero value. Although the architecture of each layer and the generating Hamiltonian is the same among all layers, the layers differ in the angles θ_{mk} as shown in Fig. 1(b).

There are also several additional modes of operation for Algorithm 1. In the first mode we already explored, we reset the circuit randomly in each run irrespective of whether the intermediate measurement succeeds, as shown in the top panel of Fig. 1(c). The resulting distribution is described by a circuit-averaged density matrix $\tilde{\rho}_{\beta,d} = \mathbb{E}_\Theta[P_{\beta,d} \rho_{\beta,d}] / \mathbb{E}_\Theta[P_{\beta,d}]$, where Θ is the full set of random angles,

$$\Theta := \{\theta_{mk} : 1 \leq m \leq M \text{ and } 1 \leq k \leq d\}. \quad (6)$$

In the second mode, we randomize the circuit only if the circuit accepts (i.e., all ancilla qubits return zero). The circuit output is simply the expectation of the accepted output density matrices $\mathbb{E}_\Theta[\rho_{\beta,d}]$. This mode requires less circuit updates and, therefore, fewer rounds of communication with the device. Finally, mode three utilizes fixed angles Θ during the entire computation as shown in the bottom panel of Fig. 1(c).

The following theorem quantifies the rate of convergence of the output of the quantum circuit to the Gibbs state (see Supplement Section ID for the proof).

Theorem 1 Let $\xi := \beta^2 M/d < 1$ be small, and define $A := M^{-1} \sum_{m=1}^M \langle h_m^2 \rangle_\beta (1 + O(\xi))$ and $C := M^{-1} \sum_{m=1}^M \text{Var}_\beta(h_m) (1 + O(\xi))$. Then for any $0 < \epsilon \leq 1$, the output of Algorithm 1 after d cycles satisfies

$$\text{mode 1: } S(\rho_\beta \| \tilde{\rho}_{\beta,d}) \leq \xi A, \quad (7)$$

$$\text{mode 2: } S(\rho_\beta \| \mathbb{E}_\Theta[\rho_{\beta,d}]) \leq \xi C, \quad (8)$$

$$\text{mode 3: } \text{Prob}\left(S(\rho_\beta \| \rho_{\beta,d}) \geq \frac{\xi C}{\epsilon}\right) \leq \epsilon, \quad (9)$$

where $S(\rho \| \sigma)$ is the relative entropy.

Theorem 1 implies that all modes require the minimum circuit depth $d \sim O(n\beta^2/\epsilon)$ to approximate the Gibbs state for typical many-body Hamiltonian within ϵ -error in the relative entropy. We also note that mode 3 samples from a distribution that is close to the thermal with probability close to unity, as stated in Eq. (9). In this case, the angle selection can be utilized to further reduce the errors when the depth is shallow and circuit is noisy, as we will show below.

In general, Algorithm 1 applies to arbitrary Hamiltonians but requires exponential time to be implemented because of the post-selection step. Nevertheless, it may serve as a subroutine to other algorithms for preparation of Gibbs states whose subsystems each have a small number of qubits. Below, we consider another randomized algorithm that prepares thermal states more efficiently but for a subclass of physical Hamiltonians.

Algorithm 2. Our second algorithm utilizes continuous time dynamics with the ancilla serving as a “digital bath”. In contrast to the previous works [15, 39], we exploit the randomness of the constructed circuit and the ancilla “bath”. We then show that this in combination with ergodicity of the Hamiltonian leads to an efficient thermal state preparation. Further we explore the option of tuning the initially random parameters of the local Hamiltonian to mitigate errors as to fight back noise in the course of the computation. We remark that Algorithm 2 does *not* require post-selection rendering its performance more efficient.

As before, the n -qubit initial state is initialized to a random state (e.g., a random product state suffices). The algorithm is cyclic. In each cycle k , and for each ancilla qubit m , we pick a random frequency ω_{mk} and assign the single-qubit Hamiltonian $B_m^{[k]} = \frac{1}{2}\omega_{mk}Z_m$ to the m -th ancilla, where Z_m is the Pauli matrix. We then randomly set the state of the ancilla to $|0\rangle$ or $|1\rangle$ according to the thermal distribution for $B_m^{[k]}$, whose respective probabilities are $p_x = 1/[1 + \exp((-1)^x \beta \omega_{mk})]$, where $x \in \{0, 1\}$.

The system and ancilla evolve continuously during the rest of the cycle. We use the following Hamiltonian to generate a unitary time evolution over a randomly chosen

time interval t_k (see below for details),

$$H^{[k]} = H \otimes I_A + \sum_{m=1}^{n_a} I_S \otimes B_m^{[k]} + \lambda \sum_{m=1}^{n_a} I_C \otimes V_{q(m)}^{[k]} \otimes X_m, \quad (10)$$

where H is the Hamiltonian for which we prepare the thermal state, I_A and I_S are identities on the system and ancilla qubits respectively. In the third term, λ is a coupling parameter, $V_{q(m)}^{[k]}$ are (random) Hermitian local operators acting on the system qubit $q(m) \in \{1, \dots, n\}$, X_m is the Pauli matrix on the m -th ancilla qubit and I_C is the identity matrix acting on the remaining qubits.

To explain the convergence of the output to the Gibbs thermal state, we study the algorithm’s performance by assuming the ETH random matrix ansatz [41, 43]. Since $V_{q(m)}^{[k]}$ are *local* operators and we are working under the ETH assumption, we have

$$\langle \mu | V_{q(m)}^{[k]} | \nu \rangle = V_{mk}(E_\mu) \delta_{\mu\nu} + \sigma_{\mu\nu}^{mk} R_{\mu\nu}^{mk}, \quad (11)$$

where E_μ and $|\mu\rangle$ are the energy and eigenstate of the Hamiltonian respectively, R^{mk} is a random matrix from the Gaussian unitary ensemble (GUE), $V_{mk}(E_\mu)$ is a slowly varying smooth function of E_μ . Lastly, denoting by $\bar{E} = (E_\mu + E_\nu)/2$, $\sigma_{\mu\nu}^{mk} = e^{-S(\bar{E})/2} f_{mk}(\bar{E}, \Omega_{\mu\nu})$, where $S(\bar{E})$ is the thermodynamic entropy and $f_{mk}(\bar{E}, \Omega_{\mu\nu})$ is the spectral function that is a slow and smooth function of the average energy \bar{E} and energy difference $\Omega_{\mu\nu} = E_\mu - E_\nu$. Because the thermodynamic entropy is extensive in the system size, the off-diagonal elements decay exponentially. The standard ETH random matrix ansatz is indeed a simplifying assumption for the behavior of the eigenstates of local quantum Hamiltonians [49]. Assuming ETH enables us to analytically quantify the performance of our algorithm.

Let us focus now on the regime of small λ and consider frequencies ω_{mk} to be sampled uniformly at random from $[-\Omega, \Omega]$, and the time intervals t_k to be a random variable from the Poisson distribution $g(t; \gamma) = \gamma \exp(-\gamma t)$. We take $\gamma \gg n_a \lambda^2 / \Omega$ where n_a is the number of ancilla qubits. Then, the expected output $\mathbb{E}[\rho_d]$ of Algorithm 2 is approximately equal to the state $\rho_d^m = \sum_\mu p_{d\mu} |\mu\rangle \langle \mu|$, where expectation is taken with respect to all randomness R^{mk} , t_k , ω_{mk} , and probabilities $p_{d\mu}$ are obtained from the solution of the following stochastic process

$$p_{k+1\mu} = (1 - \tau_\mu^k) p_{k\mu} + \sum_\nu T_{\mu\nu}^k p_{k\nu}, \quad (12)$$

with initial state $p_{0\mu} = 2^{-n}$, $\tau_\mu^k = \sum_\nu T_{\mu\nu}^k$, and transition amplitudes

$$T_{\mu\nu}^k = \frac{2\pi\lambda^2}{\gamma\Omega(1 + e^{\beta\Omega_{\mu\nu}})} \sum_{m=1}^{n_a} |\sigma_{\mu\nu}^{mk}|^2. \quad (13)$$

This classical process is a critical part of understanding Algorithm 2. Indeed, given that matrix T^k is all-to-all connected, this process converges uniquely to the

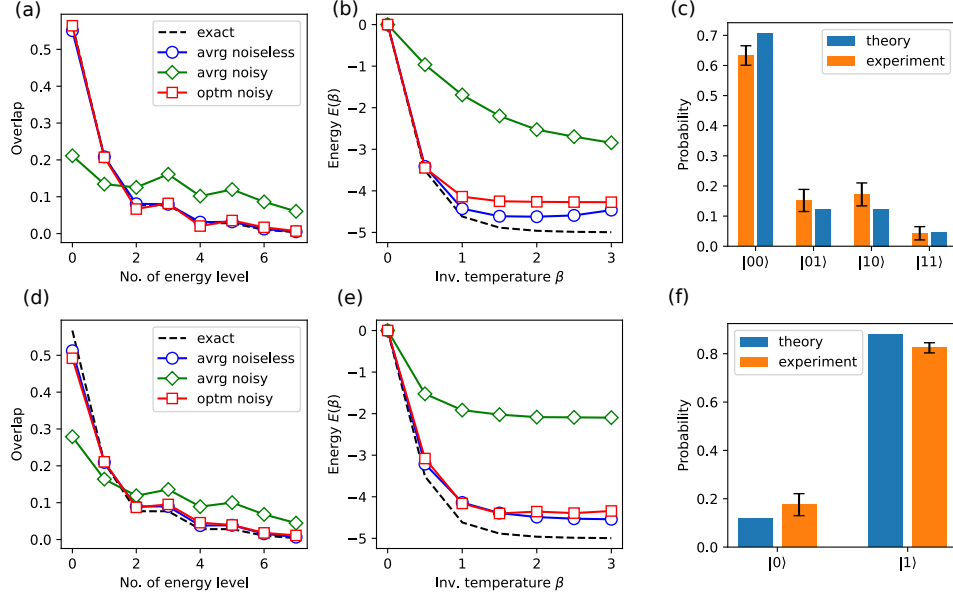


FIG. 2. Simulations and IBMQ experiments. (a)-(b) Simulation results for Algorithm 1 utilizing $n_a = 2$ ancilla qubits for 3-qubit Hamiltonian in Eq. (15), $J_{12}^x = J_{23}^x = 1$ for $\alpha = x, y, z$ and $\mu_i = -1$ (see corresponding circuit in Fig. 1(b)). The inverse temperature is $\beta = 1$ and number of cycles is $d = 5$. Panel (a) shows the overlap between expected output state in Eq. (3) and the eigenstates of the Hamiltonian for noiseless circuit (blue circles), noisy circuit (green diamonds), noisy optimized circuit (red squares), and exact solution (dashed line). We use a depolarizing noise model with single-qubit error probability $p_2 = 0.01$ for 2-qubit gates and $p_3 = 0.02$ for 3-qubit gates. An averaged circuit output is computed for 10^3 successful sample runs. (b) Output state energy as a function of temperature for the same setting as the panel (a). (c) Output probabilities in z -basis for experiment on IBM quantum hardware utilizing $n = 2$ system qubits and $n_a = 3$ ancilla qubits, $J_{12}^x = 1$, $J_{12}^y = J_{12}^z = 0$, $\mu_i = -1$. The experiment is performed on IBM 7-qubit *ibm_casablanca* device. Experiment uses 100 random circuit configurations with 8192 samples per circuit. (d)-(e) Performance for Algorithm 2 for the same setting as Panel (a)-(b), except using $d = 20$ cycles, $\gamma = 0.1$, and single-qubit depolarizing error probability $p = \Gamma t$ after each cycle, where t is the cycle time and $\Gamma = 10^{-3}$. The average is based on 10^3 sample runs. (c) Experiment for Algorithm 2 for $n = 1$ system qubit and $n_a = 1$ ancilla qubit, implemented on *ibm_casablanca* device with Hamiltonian $H = Z$. This Panel shows the output probabilities in z -basis. The coupling is $\lambda = 0.1$ for the first cycle and it decreases linearly with number of cycles, $\gamma = 0.01$, a_{mk} and b_{mk} are generated from standard normal distribution. Experiment uses 150 random circuit configurations with 8192 samples per circuit.

Gibbs state $p_{\infty\mu} \propto \exp(-\beta E_\mu)$ as a result of detailed balance condition, $T_{\mu\nu}^k/T_{\nu\mu}^k = \exp(-\beta\Omega_{\mu\nu})$. Notably, after d steps the process in Eq. (12) generates only $D = O(d\gamma\Omega/n_a\lambda^2)$ successful transitions. As such, D is an essential parameter since it controls the convergence of the algorithm to the steady state. Using this parameter, the distance of the output of Algorithm 2 to the density matrix ρ_d^m generated the stochastic process in Eq. (12) is quantified in the following theorem:

Theorem 2 Let $c > 1$ be a constant and take $\Omega = c\|H\| > \beta^{-1}$, the depth $d = O(D^2)$, and number of ancilla qubits $n_a = O(\beta D\|H\|)$. For any $0 < \epsilon \leq 1$, set $\lambda = O(\sqrt{\epsilon}/\beta D^{3/2})$ and $\gamma = O(\epsilon/\beta D)$. Then we have

$$\delta(\mathbb{E}[\rho_d] | \rho_\beta) \leq \delta(\rho_d^m | \rho_\beta) + O(\epsilon), \quad (14)$$

where $\delta(\sigma|\rho)$ is trace distance.

In this Theorem, depth d is selected to ensure that the process produces $O(D)$ successful transitions. Algorithm 2 is therefore always comparable to the D -step

Metropolis algorithm in accordance with the theorem. The average time of preparing the thermal state would scale as $t \propto \gamma^{-1}d = O(\beta D^3/\epsilon)$, where the scaling of D with the system size depends on the Hamiltonian structure. Thus, whenever quantum Metropolis algorithm requires polynomial resources, then Algorithm 2 is also a polynomial-time algorithm.

Simulations and IBMQ experiments. We illustrate the performance of the algorithms using the 2-local Hamiltonian

$$H = \sum_{\alpha=1}^3 \sum_{i<j}^n J_{ij}^\alpha S_i^\alpha S_j^\alpha + \sum_{i=1}^n \mu_i Z_i, \quad (15)$$

where $S^\alpha = \{X^\alpha, Y^\alpha, Z^\alpha\}$ is the set of Pauli matrices and J_{ij}^α are couplings between qubits, μ_i are single-qubit coefficients. This Hamiltonian encompasses a broad class of interesting models. For example, in one-dimension and with $J_{i,i+1}^x = J_{j,j+1}^y = J$, $\mu_i = -J_{i,i+1}^z = \mu$, it becomes the celebrated Fermi-Hubbard model that cap-

tures interaction-induced phenomena such as the metal-insulator transition [50]. The Hamiltonian in Eq. (15) models exotic spin liquid states [51] and rich phenomena in quantum criticality [52]. We comment that for Hamiltonians with local Pauli terms, Algorithm 1 becomes more efficient: A CNOT gate plus single qubit gates can implement any 2-qubit gate in Eq. (2) that connects a system qubit with a qubit in the ancilla. Further, a three-qubit gate that interacts two of the system's qubits with a qubit in the ancilla can be implemented with just two CNOT gates plus single qubit gates (see Supplement Section IF for details).

We measure the performance of the algorithms by computing the overlaps between the simulated output state and the Hamiltonian eigenstates and then compare that to the overlaps between eigenstates and the ideal Gibbs thermal state. Fig. 2(a) shows such comparison for Algorithm 1 applied to noiseless and noisy circuits. While noiseless circuits give accurate results, the noise inevitably degrades the accuracy of thermal state preparation by increasing the overall state entropy. To study the dependence of the errors on temperature, we show the dependence of the state energy $E = \text{Tr}(\tilde{\rho}_{\beta,d}H)$ as a function of temperature by comparing it to the exact thermal values $\langle H \rangle_{\beta}$ in Fig. 2(b). Evidently, the performance of the algorithm at high temperatures is better than the low temperatures. Fig. 2(d,e) show similar dependencies for Algorithm 2. Both algorithms were implemented on the latest version of IBM quantum hardware; we run the algorithms on Qiskit for small devices, as shown in Fig 2(c,f).

Noise and error mitigation. For both algorithms, the error can be reduced by adjusting circuit parameters (gate angles or Hamiltonian parameters). Using the same parameters for each sampling run and adjusting them to minimize the output's free energy, better precision can be achieved. In practice, such an optimization utilizes a classical computer, similar to existing variational quantum algorithms. In this scheme, the classical computer uses readings from the circuit output and has the power to adjust the parameters of the circuit for the next run to achieve better performance, see Fig. 1(b,d). By utilizing such feedback loop we effectively perform error mitigation.

It is worth emphasizing that these algorithms have advantages over variational algorithms beyond just providing provable guarantees. In particular, a typical noiseless circuit must return an output state which is ϵ -close to the target state; this significantly reduces the barren plateau problem. Even in the presence of noise, when such ϵ -closeness is hard to prove, we empirically observe that random configurations are suitable good ansatz.

To mitigate errors in Algorithm 1, we optimize over random gate angles θ_{mk} . Fig. 2(a) shows a significant improvement compared to average-case scenario for the Hamiltonian in Eq. (15). Also, Fig. 2(b) shows that the thermal state energy as a function of temperature

also improves, with better performance at higher temperatures. We use a similar optimization for Algorithm 2, with results shown in Fig. 1(d,e). For simplicity, we look into parametrized family of local operators $V^{(mk)} = a_{mk}X_m + b_{mk}Z_m$, where a_{mk}, b_{mk} are real numbers. Thus, the circuit can further be adjusted over the set $\mathcal{T} = \{t_k, \omega_{mk}, a_{mk}, b_{mk}\}$. We start from an arbitrary choice of these parameters. To get faster convergence we start with larger values of a_{mk} and b_{mk} to take larger steps towards the Gibbs state and then decrease them with k to converge to the optimal (not unlike the adaptive gradient descent). The resulting occupation of energy levels in Fig. 2(c) exhibits significant improvement compared to the noisy case. Fig. 2(b) illustrates the performance for different temperatures and as can be seen the performance improves with increasing temperature (similar to noiseless case).

Conclusions and outlook. We proposed two quantum algorithms that take advantage of random quantum circuits to prepare thermal Gibbs states. These algorithms are amenable to further improvements. For example, $O(1)$ -temperature Gibbs states for one-dimensional classical Hamiltonians allow sampling in polynomial time by combining Algorithm 1 and merging technique proposed in [17], which also reduce required resources in higher dimensions. Further, the error associated with finite depth in Algorithm 1 could be reduced by using higher-order product formulas [14] and randomized gate positions [53]. Both algorithms may be improved by more refined implementations such as layer-by-layer optimization [54] and supervised machine learning for optimizing circuit parameters.

In Algorithm 2, local Hamiltonian evolution is required, which can currently be performed on existing quantum simulation devices. Nevertheless, for digital quantum computing platforms, continuous-time dynamics remains challenging since it requires a minimum number of $O(n/\gamma)$ trotterized circuit layers at each cycle in order to achieve a desirable degree of precision [14]. On the other hand, periodically-driven (Floquet) systems can be simulated more effectively using digital devices. Thus, using Algorithm 2, it is possible to prepare quasi-thermal states for Floquet Hamiltonians, including topological states with zero quasienergy [55]. We leave a thorough investigation of this for future work.

While preparing this manuscript, we became aware of [56], which similar to our Theorem 2 shows that ETH indeed implies fast thermalization to the Gibbs state.

Available Code. The code used to generate presented data is available at:

<https://github.com/IBM/gibbs-qalgrthms>

Acknowledgements. – We would like to thank David Layden, Sarah Sheldon, Mario Motta, Jeff Cohn, Kunal Sharma, Abhinav Deshpande, and Kristan Temme for helpful discussions. We acknowledge funding from the

-
- [1] D. Poulin and P. Wocjan, Sampling from the thermal quantum gibbs state and evaluating partition functions with a quantum computer, *Phys. Rev. Lett.* **103**, 220502 (2009).
- [2] A. Riera, C. Gogolin, and J. Eisert, Thermalization in nature and on a quantum computer, *Phys. Rev. Lett.* **108**, 080402 (2012).
- [3] K. Temme, T. J. Osborne, K. G. Vollbrecht, D. Poulin, and F. Verstraete, Quantum metropolis sampling, *Nature* **471**, 87 (2011).
- [4] M.-H. Yung and A. Aspuru-Guzik, A quantum-quantum metropolis algorithm, *P. Natl. Acad. Sci.* **109**, 754 (2012).
- [5] M. Cerezo, A. Arrasmith, R. Babbush, S. C. Benjamin, S. Endo, K. Fujii, J. R. McClean, K. Mitarai, X. Yuan, L. Cincio, and P. J. Coles, Variational quantum algorithms, *Nat. Rev. Phys.* **3**, 625 (2021).
- [6] J. Wu and T. H. Hsieh, Variational thermal quantum simulation via thermofield double states, *Phys. Rev. Lett.* **123**, 220502 (2019).
- [7] G. Verdon, J. Marks, S. Nanda, S. Leichenauer, and J. Hidary, Quantum hamiltonian-based models and the variational quantum thermalizer algorithm, *arXiv:1910.02071* (2019).
- [8] B. Bauer, S. Bravyi, M. Motta, and G. K.-L. Chan, Quantum algorithms for quantum chemistry and quantum materials science, *Chem. Rev.* **120**, 12685 (2020).
- [9] W. Hofstetter and T. Qin, Quantum simulation of strongly correlated condensed matter systems, *J. Phys. B - At. Mol. Opt.* **51**, 082001 (2018).
- [10] U.-J. Wiese, Ultracold quantum gases and lattice systems: quantum simulation of lattice gauge theories, *Ann. Phys.-Berlin* **525**, 777 (2013).
- [11] R. D. Somma, S. Boixo, H. Barnum, and E. Knill, Quantum simulations of classical annealing processes, *Phys. Rev. Lett.* **101**, 130504 (2008).
- [12] E. Y. Loh, J. E. Gubernatis, R. T. Scalettar, S. R. White, D. J. Scalapino, and R. L. Sugar, Sign problem in the numerical simulation of many-electron systems, *Phys. Rev. B* **41**, 9301 (1990).
- [13] I. M. Georgescu, S. Ashhab, and F. Nori, Quantum simulation, *Rev. Mod. Phys.* **86**, 153 (2014).
- [14] A. M. Childs and Y. Su, Nearly optimal lattice simulation by product formulas, *Phys. Rev. Lett.* **123**, 050503 (2019).
- [15] B. M. Terhal and D. P. DiVincenzo, Problem of equilibration and the computation of correlation functions on a quantum computer, *Phys. Rev. A* **61**, 022301 (2000).
- [16] J. E. Moussa, Measurement-based quantum metropolis algorithm, *arXiv:1903.01451* (2019).
- [17] E. Bilgin and S. Boixo, Preparing thermal states of quantum systems by dimension reduction, *Phys. Rev. Lett.* **105**, 170405 (2010).
- [18] A. N. Chowdhury and R. D. Somma, Quantum algorithms for gibbs sampling and hitting-time estimation, *Quantum Info. Comput.* **17**, 41–64 (2017).
- [19] J. R. McClean, S. Boixo, V. N. Smelyanskiy, R. Babbush, and H. Neven, Barren plateaus in quantum neural network training landscapes, *Nat. Comm.* **9**, 4812 (2018).
- [20] M. Motta, C. Sun, A. T. Tan, M. J. O’Rourke, E. Ye, A. J. Minnich, F. G. Brandão, and G. K. L. Chan, Determining eigenstates and thermal states on a quantum computer using quantum imaginary time evolution, *Nature Physics* **16**, 205 (2020).
- [21] S.-N. Sun, M. Motta, R. N. Tazhigulov, A. T. Tan, G. K.-L. Chan, and A. J. Minnich, Quantum computation of finite-temperature static and dynamical properties of spin systems using quantum imaginary time evolution, *PRX Quantum* **2**, 010317 (2021).
- [22] A. Shabani and H. Neven, Artificial quantum thermal bath: Engineering temperature for a many-body quantum system, *Phys. Rev. A* **94**, 052301 (2016).
- [23] Y. Ashida, K. Saito, and M. Ueda, Thermalization and heating dynamics in open generic many-body systems, *Phys. Rev. Lett.* **121**, 170402 (2018).
- [24] H.-Y. Su and Y. Li, Quantum algorithm for the simulation of open-system dynamics and thermalization, *Phys. Rev. A* **101**, 012328 (2020).
- [25] M. Metcalf, J. E. Moussa, W. A. de Jong, and M. Sarovar, Engineered thermalization and cooling of quantum many-body systems, *Phys. Rev. Research* **2**, 023214 (2020).
- [26] L. J. Schulman, T. Mor, and Y. Weinstein, Physical limits of heat-bath algorithmic cooling, *Phys. Rev. Lett.* **94**, 120501 (2005).
- [27] E. Kapit, Universal two-qubit interactions, measurement, and cooling for quantum simulation and computing, *Phys. Rev. A* **92**, 012302 (2015).
- [28] A. E. Allahverdyan, R. S. Gracià, and T. M. Nieuwenhuizen, Bath-assisted cooling of spins, *Phys. Rev. Lett.* **93**, 260404 (2004).
- [29] T. Zhou and A. Nahum, Entanglement membrane in chaotic many-body systems, *Phys. Rev. X* **10**, 031066 (2020).
- [30] A. Lavasani, Y. Alavirad, and M. Barkeshli, Measurement-induced topological entanglement transitions in symmetric random quantum circuits, *Nat. Phys.* **17**, 342 (2021).
- [31] R. Movassagh, Quantum supremacy and random circuits, *arXiv:1909.06210* (2019).
- [32] Y. Kondo, R. Mori, and R. Movassagh, Improved robustness of quantum supremacy for random circuit sampling, *arXiv:2102.01960* (2021).
- [33] A. Bouland, B. Fefferman, C. Nirkhe, and U. Vazirani, On the complexity and verification of quantum random circuit sampling, *Nat. Phys.* **15**, 159 (2019).
- [34] S. Hallgren, D. Nagaj, and S. Narayanaswami, The local hamiltonian problem on a line with eight states is qma-complete, *Quantum Info. Comput.* **13**, 721–750 (2013).
- [35] D. Aharonov, D. Gottesman, S. Irani, and J. Kempe, The power of quantum systems on a line, *Comm. Math. Phys.* **287**, 41 (2009).
- [36] N. Schuch, M. M. Wolf, F. Verstraete, and J. I. Cirac, Computational complexity of projected entangled pair states, *Phys. Rev. Lett.* **98**, 140506 (2007).

- [37] S. Piddock and A. Montanaro, The complexity of antiferromagnetic interactions and 2d lattices, *Quantum Info. Comput.* **17**, 636–672 (2017).
- [38] J. Bausch, T. Cubitt, and M. Ozols, The complexity of translationally invariant spin chains with low local dimension, *Annales Henri Poincaré* **18**, 3449 (2017).
- [39] S. Polla, Y. Herasymenko, and T. E. O’Brien, Quantum digital cooling, *Phys. Rev. A* **104**, 012414 (2021).
- [40] J. M. Deutsch, Quantum statistical mechanics in a closed system, *Phys. Rev. A* **43**, 2046 (1991).
- [41] M. Srednicki, The approach to thermal equilibrium in quantized chaotic systems, *J. Phys. A-Math. Gen.* **32**, 1163 (1999).
- [42] M. Srednicki, Chaos and quantum thermalization, *Phys. Rev. E* **50**, 888 (1994).
- [43] L. D’Alessio, Y. Kafri, A. Polkovnikov, and M. Rigol, From quantum chaos and eigenstate thermalization to statistical mechanics and thermodynamics, *Adv. Phys.* **65**, 239 (2016).
- [44] J. M. Deutsch, Eigenstate thermalization hypothesis, *Rep. Prog. Phys.* **81**, 082001 (2018).
- [45] M. Rigol, V. Dunjko, and M. Olshanii, Thermalization and its mechanism for generic isolated quantum systems, *Nature* **452**, 854 (2008).
- [46] D. Levin and Y. Peres, *Markov Chains and Mixing Times*, MBK (American Mathematical Society, 2017).
- [47] T. Liu, J.-G. Liu, and H. Fan, Probabilistic nonunitary gate in imaginary time evolution, *Quantum Inf. Process.* **20**, 1 (2021).
- [48] A. M. Childs, Y. Su, M. C. Tran, N. Wiebe, and S. Zhu, Theory of trotter error with commutator scaling, *Phys. Rev. X* **11**, 011020 (2021).
- [49] A. Dymarsky, Bound on eigenstate thermalization from transport, *arXiv:1804.08626* (2018).
- [50] M. Imada, A. Fujimori, and Y. Tokura, Metal-insulator transitions, *Rev. Mod. Phys.* **70**, 1039 (1998).
- [51] Y. Zhou, K. Kanoda, and T.-K. Ng, Quantum spin liquid states, *Rev. Mod. Phys.* **89**, 025003 (2017).
- [52] S. Suzuki, J. Inoue, and B. Chakrabarti, *Quantum Ising Phases and Transitions in Transverse Ising Models*, Lecture Notes in Physics (Springer Berlin Heidelberg, 2012).
- [53] E. Campbell, Random compiler for fast hamiltonian simulation, *Phys. Rev. Lett.* **123**, 070503 (2019).
- [54] A. Skolik, J. R. McClean, M. Mohseni, P. van der Smagt, and M. Leib, Layerwise learning for quantum neural networks, *Quantum Mach. Intell.* **3**, 1 (2021).
- [55] V. Khemani, A. Lazarides, R. Moessner, and S. L. Sondhi, Phase structure of driven quantum systems, *Phys. Rev. Lett.* **116**, 250401 (2016).
- [56] C.-F. Chen and F. G. Brandão, Fast thermalization from the eigenstate thermalization hypothesis, *arXiv:2112.07646* (2021).
- [57] J. Zhang, J. Vala, S. Sastry, and K. B. Whaley, Exact two-qubit universal quantum circuit, *Phys. Rev. Lett.* **91**, 027903 (2003).

Supplemental Material: “Algorithms for Gibbs state preparation on noiseless and noisy random quantum circuits”

Oles Shtanko¹ and Ramis Movassagh²

¹*IBM Quantum, IBM Research, Almaden, San Jose CA, 95120, USA*

²*IBM Quantum, MIT-IBM Watson AI lab, Cambridge MA, 02142, USA*

CONTENTS

| | | |
|-----|--|----|
| I. | Details of Algorithm 1 | S1 |
| | A. Quasi-thermal distribution in Eq. (4) | S1 |
| | B. Error scaling in Eq. (5) | S2 |
| | C. Success probability | S2 |
| | D. Proof of Theorem 1 | S3 |
| | E. Simulation of Algorithm 1 | S4 |
| | F. Optimized gate implementation | S5 |
| II. | Details of Algorithm 2 | S5 |
| | A. Proof of Theorem 2 | S5 |
| | B. Proof of Lemma 3 | S8 |

I. DETAILS OF ALGORITHM 1

In this section, we analyze the performance of Algorithm 1. It contains three basic steps: randomizing the angles by choosing $\theta_{mk} \in \mathcal{N}(0, 1)$, running the circuit for a random initial state (which can be taken to be a random product state), and measuring the outcome. If all intermediate ancilla measurements return zero, the circuit accepts; otherwise rejects the output and the circuit is re-run. Once the circuit accepts, we obtain a bit string by measuring the qubits and repeat the procedure to obtain another sample. There are three modes of implementing the algorithm in the sampling loop, as shown in Fig 1(c). In the first mode ($\alpha = 1$), the circuit is randomized every time we run it regardless of the acceptance or rejection of the circuit. This way we obtain circuit-averaged outcome of the form $\tilde{\rho}_{\beta,d} \propto \mathbb{E}_{\Theta} P[\Theta] \rho[\Theta]$, where $P_{\beta,d}[\Theta]$ is the probability of acceptance and $\rho[\Theta]$ is the postselected output density matrix. In the second mode ($\alpha = 2$), we randomize the circuit only if the circuit accepts. Finally, in the third mode ($\alpha = 3$), we fix the randomly generated circuit angles for the entire computation process. The latter gives us a circuit-specific outcome, $\rho_{\text{out}} = \rho[\Theta]$.

Our current work utilizes all three modes of Algorithm 1. For example, the averaged simulated curves in Fig. 2(a,b,d,e) in the main text are computed in mode 1. The optimized curves on the same plots, however, require the use of fixed gate angles throughout the experiment, which is equivalent to mode 3. Finally, IBMQ experi-

ments are conducted using mode 2 because it requires fewer communication rounds with the device.

A. Quasi-thermal distribution in Eq. (4)

Here we evaluate the thermal distribution in Eq. (4) in the main text that is obtained using mode 1 ($\alpha = 1$). This distribution is a particular case of the Algorithm for the number of ancilla qubits $n_a = 1$. We recall that Algorithm 1 can be performed by a series of d gates, where for each $k \in \{1, 2, \dots, d\}$

$$U(\theta_k, H) = \exp\left(i\theta_k \sqrt{\beta H/d} \otimes X\right), \quad (\text{S.1})$$

where X applies to ancilla qubit. This operation is followed by the measurement of the ancilla qubit and postselection. Let $\rho_{\beta,k}$ be the postselected output of k -th gate, and set $|\Psi_0\rangle = |\psi\rangle|0\rangle$ as the initial state. Then, the first gate results in:

$$\begin{aligned} |\Psi_1\rangle := U(\theta_1, H)|\Psi_0\rangle &= \cos(\theta_1 \sqrt{\beta H/d}) |\psi\rangle|0\rangle \\ &\quad + i \sin(\theta_1 \sqrt{\beta H/d}) |\psi\rangle|1\rangle. \end{aligned} \quad (\text{S.2})$$

Algorithm 1**Input**

$\alpha \in \{1, 2, 3\}$ (mode index)
 $L \geq 1$ (number of samples)
 $d \geq 1$ (circuit depth)
 $h_m, m \in 1 \dots M$ (Hamiltonian terms)

Output

S (qubit measurements outcomes)

if $\alpha = 3$ **then**

set $\{\theta_{mk}\}, \theta_{mk} \in \mathcal{N}(0, 1)$

end if

$l = 1$

while $l \leq L$ **do**

$s = 1$

if $\alpha = 2$ **then**

set $\{\theta_{mk}\}, \theta_k \in \mathcal{N}(0, 1)$

end if

$k = 1$

$m = 1$

while $k \leq d$ **do****while** $m \leq M$ **do****if** $s = 0$ **then**

$|\psi\rangle \leftarrow U(\theta_k, \beta H/d)|\psi\rangle$
measure ancilla, $s \leftarrow \text{result}$
 $k = k + 1$

else**if** $\alpha = 1$ **then**

set $\{\theta_{mk}\}, \theta_k \in \mathcal{N}(0, 1)$

end if

$|\psi\rangle = |r\rangle \otimes |0\rangle, r \in \mathbb{C}_2^n$

$k = 1$

$s = 0$

end if**end while****end while**

measure qubits, add to S

end while

Let us define $r_{\beta,d} = \mathbb{E}[P_{\beta,d}\rho_{\beta,d}]$, where $P_{\beta,d}$ is the probability of circuit acceptance. The outcome of the first gate, upon averaging the angle, and post-selecting on $|0\rangle_A$ which below we simply denote by $|0\rangle$ gives

$$\begin{aligned} r_{\beta,1} &:= \langle 0 | \mathbb{E}_{\theta_1, \psi} | \Psi_1 \rangle \langle \Psi_1 | | 0 \rangle = \frac{1}{2^n} \mathbb{E}_{\theta_1} \cos^2(\theta_1 \sqrt{\beta H/d}) \\ &= \frac{1}{2^{n+1}} \mathbb{E}_{\theta_1} \left[I + \cos(2\theta_1 \sqrt{\beta H/d}) \right] \\ &= \frac{1}{2^{n+1}} \left[I + \exp(-2\beta H/d) \right]. \end{aligned} \quad (\text{S.3})$$

Iterating this procedure, it is straightforward to show that the density matrix after d gates take the form

$$r_{\beta,d} = \frac{1}{2^{n+d}} \left[I + \exp(-2\beta H/d) \right]^d \quad (\text{S.4})$$

Using binomial decomposition and normalizing the outcome, we arrive at

$$\rho_{\beta,d} = \frac{1}{\mathcal{Z}_{\beta,d}} \sum_{k=0}^d \binom{d}{k} \exp(-\beta_k H), \quad (\text{S.5})$$

where $\beta_k = 2\beta k/d$ and $\mathcal{Z}_{\beta,d} = \sum_{\mu} e^{-\beta E_{\mu}} \cosh^d(\beta E_{\mu}/d)$ is modified partition function, and E_{μ} is the spectrum of Hamiltonian H . This proves Eq. (4) in the main text.

B. Error scaling in Eq. (5)

We now derive the asymptotic behaviour for the error, where d^{-1} is the small parameter. We use the expansion

$$\begin{aligned} \tilde{\rho}_{\beta,d} &\propto \exp(-\beta H) \cosh^d(\beta H/d) \\ &= \exp\left(-\beta H + \frac{\beta^2 H^2}{2d} + O\left(\frac{1}{d^2}\right)\right), \end{aligned} \quad (\text{S.6})$$

The convergence of this state to the Gibbs state ρ_{β} is established as follows:

Lemma 1 Consider density operator

$$\rho'_{\beta} = \frac{1}{\mathcal{Z}'} e^{-\beta(H+\lambda V)}, \quad (\text{S.7})$$

where $\mathcal{Z}' = \text{Tr } e^{-\beta(H+\lambda V)}$, V is Hermitian operator and λ is a small parameter. Then

$$S(\rho_{\beta} \| \rho'_{\beta}) \leq \frac{1}{2} \lambda^2 \beta^2 (\langle V^2 \rangle_{\beta} - \langle V \rangle_{\beta}^2) + O(\lambda^3). \quad (\text{S.8})$$

Proof of Lemma 1. We express

$$\begin{aligned} S(\rho_{\beta} \| \rho'_{\beta}) &= \langle \log \rho_{\beta} - \log \rho'_{\beta} \rangle_{\beta} \\ &= -\log \mathcal{Z} + \lambda \beta \langle V \rangle_{\beta} + \log \text{Tr } e^{-\beta(H+\lambda V)}. \end{aligned} \quad (\text{S.9})$$

Using Golden-Thompson inequality, we get

$$\begin{aligned} S(\rho_{\beta} \| \rho'_{\beta}) &\leq \lambda \beta \langle V \rangle_{\beta} + \log \mathcal{Z}^{-1} \text{Tr } e^{-\beta H} e^{-\lambda \beta V} \\ &= \lambda \beta \langle V \rangle_{\beta} + \log \langle e^{-\lambda \beta V} \rangle_{\beta}. \end{aligned} \quad (\text{S.10})$$

Using the Taylor expansion, we get

$$\log \langle e^{-\lambda \beta V} \rangle_{\beta} = -\lambda \beta \langle V \rangle_{\beta} + \frac{1}{2} \lambda^2 \beta^2 (\langle V^2 \rangle_{\beta} - \langle V \rangle_{\beta}^2) + O(\lambda^3). \quad (\text{S.11})$$

Substituting this into Eq. (S.10), proves the Lemma. \square

Using Eq. (S.6) and Lemma 1, where $\lambda = d^{-1}$ and $V = \beta^2 H^2/2 + O(d^{-1})$, we get

$$S(\rho_{\beta} \| \tilde{\rho}_{\beta,d}) \leq \frac{\beta^4}{8d^2} (\langle H^4 \rangle_{\beta} - \langle H^2 \rangle_{\beta}^2) + O\left(\frac{1}{d^3}\right). \quad (\text{S.12})$$

This expression gives us the asymptotic behaviour of the error in Eq. (5) in the main text.

C. Success probability

The circuit results must be accepted only if all ancilla measurements return zero. The probability of such event success is determined by Eq. (S.4) as

$$P_{\beta,d} = \text{Tr } r_{\beta,d} = \frac{\mathcal{Z}_{\beta,d}}{2^n} \quad (\text{S.13})$$

where $\mathcal{Z}_{\beta,d}$ is modified partition function that satisfies

$$\mathcal{Z}_{\beta,d} := \sum_{\mu} e^{-\beta E_{\mu}} \cosh^d(\beta E_{\mu}/d) \geq \sum_{\mu} e^{-\beta E_{\mu}} = \mathcal{Z}_{\beta}. \quad (\text{S.14})$$

Therefore,

$$P_{\beta,d} \geq 2^{-\alpha n}, \quad \alpha = 1 - (\log_2 \mathcal{Z}_{\beta})/n \quad (\text{S.15})$$

Note that $\beta = 0$ corresponds to the partition function $\mathcal{Z}_{\beta} = 2^n$ for any Hamiltonian. In this case, as follows from Eq. (S.15), the success probability is $P_{\beta,d} = 1$. This observation is easily explained by noting that in the case $\beta = 0$ all the gates in the circuit are trivial and the system state is already initialized in infinite-temperature (fully mixed) state.

D. Proof of Theorem 1

We recall that the system state dynamics includes d cycles, each consisting of M gates followed by post-selected measurements of the ancilla. Let $\rho_{m,k}[\Theta]$ be the state of the system qubits after the measurement of the m -th gate in the k -th cycle, where as before $\Theta := \{\theta_{mk}\}$ denotes the dependence on the angles. And let $P_{m,k}[\Theta]$ be the probability of acceptance of the overall circuit at this stage (i.e., all ancillas till now measured to be in the zero state). Let $r_{m,k}[\Theta] := P_{m,k}[\Theta]\rho_{m,k}[\Theta]$, which for $m \geq 2$ and a given cycle k writes

$$\begin{aligned} r_{m,k}[\Theta] &= P_{m-1,k}[\Theta] \langle 0|U_{mk}(\rho_{m-1,k}[\Theta] \otimes |0\rangle\langle 0|)U_{mk}^{\dagger}|0\rangle \\ &= \Phi_m(r_{m-1,k}) \end{aligned} \quad (\text{S.16})$$

where $U_{mk} := U(\theta_{mk}, \beta h_m/d)$ is defined in Eq. (2) in the main text and we defined the map

$$\Phi_m(\star) := \cos(\theta_{km}\sqrt{\beta h_m/d})(\star) \cos(\theta_{km}\sqrt{\beta h_m/d}) \quad (\text{S.17})$$

Using this recurrence relation, we can also connect the probability-weighted state of the system at the end of the $k-1$ st cycle to the one at the beginning of the k th cycle

$$r_{M,k}[\Theta] = \Phi_M \circ \Phi_{M-1} \circ \dots \circ \Phi_1(r_{M,k-1}) \quad (\text{S.18})$$

We set the input state to be the fully mixed state, i.e. $\rho_0 = I/2^n$, where I is $2^n \times 2^n$ identity matrix. Then, the overall circuit output is

$$P_{M,d}[\Theta]\rho_{M,d}[\Theta] = \mathcal{C}[\Theta]\rho_0\mathcal{C}^{\dagger}[\Theta] = \frac{1}{2^n}\mathcal{C}[\Theta]\mathcal{C}^{\dagger}[\Theta], \quad (\text{S.19})$$

where we defined the propagator

$$\mathcal{C}[\Theta] := \prod_{k=1}^d \left(\prod_{m=1}^M \cos \theta_{mk} \sqrt{\beta h_m/d} \right). \quad (\text{S.20})$$

and $\prod_{m=1}^M$ is ordered direct product defined as $\prod_{m=1}^M a_m := a_M \dots a_1$. The asymptotic behaviour of the output state in Eq. (S.19) is given by:

Lemma 2 Assuming that d^{-1} is small,

$$\mathcal{C}[\Theta]\mathcal{C}^{\dagger}[\Theta] = \exp\left[-\beta\left(H + \frac{1}{d}V\right)\right], \quad (\text{S.21})$$

where

$$V = \sum_{m=1}^M \sum_{k=1}^d \left[(\theta_{mk}^2 - 1)h_m + \frac{\beta}{6d}\theta_{mk}^4 h_m^2 \right] + O(1). \quad (\text{S.22})$$

Proof of Lemma 2. First, we use Taylor's expansion by inverse depth d^{-1} to express

$$\begin{aligned} \cos \theta_{mk} \sqrt{\beta h_m/d} &= 1 - \frac{\beta h_m}{2d} \theta_{mk}^2 + \frac{\beta^2 h_m^2}{24d^2} \theta_{mk}^4 + O\left(\frac{1}{d^3}\right) \\ &= \exp\left[-\frac{\beta h_m}{2d} \theta_{mk}^2 - \frac{\beta^2 h_m^2}{12d^2} \theta_{mk}^4 + O\left(\frac{1}{d^3}\right)\right] \\ &= \exp\left(-\frac{\xi_{mk}}{d}\right), \end{aligned} \quad (\text{S.23})$$

where $\xi_{mk} := \beta \theta_{mk}^2 h_m / 2 + \beta^2 \theta_{mk}^4 h_m^2 / 12d + O(d^{-2})$. Using this representation, we rewrite

$$\mathcal{C}[\Theta]\mathcal{C}^{\dagger}[\Theta] = \mathcal{E}[\Theta]\mathcal{E}^{\dagger}[\Theta]. \quad (\text{S.24})$$

where

$$\mathcal{E}[\Theta] := \prod_{k=1}^d \prod_{m=1}^M \exp\left(-\frac{\xi_{mk}}{d}\right). \quad (\text{S.25})$$

Using Suzuki-Trotter product formula (see [14, 48]), we express

$$\mathcal{E}[\Theta]\mathcal{E}^{\dagger}[\Theta] = \exp\left(-\frac{2}{d} \sum_{m=1}^M \sum_{k=1}^d \xi_{mk} + O\left(\frac{1}{d}\right)\right). \quad (\text{S.26})$$

Using this result, we obtain the expression

$$\begin{aligned} \mathcal{C}[\Theta]\mathcal{C}^{\dagger}[\Theta] &= \exp\left(-\frac{\beta}{d} \sum_{m=1}^M \sum_{k=1}^d \left\{ \theta_{mk}^2 h_m + \frac{\beta}{6d} \theta_{mk}^4 h_m^2 \right\} + O\left(\frac{1}{d}\right)\right) \\ &= \exp\left[-\beta H - \frac{\beta}{d} \sum_{m=1}^M \sum_{k=1}^d \left\{ (\theta_{mk}^2 - 1)h_m + \frac{\beta}{6d} \theta_{mk}^4 h_m^2 \right\} + O\left(\frac{1}{d}\right)\right]. \end{aligned} \quad (\text{S.27})$$

This leads us to the statement of the Lemma. \square

Let us first derive the performance of the algorithm in mode 1. To do so, we first express the expected density matrix as

$$\tilde{\rho}_{\beta,d} = \mathbb{E}_{\Theta} \mathcal{C}[\Theta]\mathcal{C}^{\dagger}[\Theta] / \text{Tr} \left(\mathbb{E}_{\Theta} \mathcal{C}[\Theta]\mathcal{C}^{\dagger}[\Theta] \right) \quad (\text{S.28})$$

Using Lemma 2, we get

$$\begin{aligned} S(\rho_\beta \| \tilde{\rho}_{\beta,d}) &= \langle \rho_\beta - \tilde{\rho}_{\beta,d} \rangle_\beta \\ &= -\log \mathcal{Z}_\beta - \beta H + \log \mathbb{E}_\Theta \text{Tr} e^{-\beta(H+V/d)} \\ &\quad - \langle \log \mathbb{E}_\Theta e^{-\beta(H+V/d)} \rangle_\beta \end{aligned} \quad (\text{S.29})$$

By applying Golden-Thompson inequality to the second term and Jensen's inequality to the third term in r.h.s., we get

$$\begin{aligned} S(\rho_\beta \| \tilde{\rho}_{\beta,d}) &\leq -\log \mathcal{Z}_\beta - \beta H + \log \mathbb{E}_\Theta \text{Tr} e^{-\beta H} e^{-\beta V/d} \\ &\quad - \langle \mathbb{E}_\Theta \log e^{-\beta(H+V/d)} \rangle_\beta \\ &= \beta \langle V \rangle_\beta + \log \mathbb{E}_\Theta \langle e^{-\beta V/d} \rangle_\beta \end{aligned} \quad (\text{S.30})$$

By performing Taylor expansion, we get

$$S(\rho_\beta \| \tilde{\rho}_{\beta,d}) \leq \frac{\beta^2}{2d^2} \left(\mathbb{E}_\Theta \langle V^2 \rangle_\beta - \langle \mathbb{E}_\Theta V \rangle_\beta^2 \right) + \left(\frac{1}{d^3} \right) \quad (\text{S.31})$$

Using that $\mathbb{E}_\Theta (\theta_{mk}^2 - 1) = 0$ and $\mathbb{E}_\Theta (\theta_{mk}^2 - 1)^2 = 2$, we obtain

$$\mathbb{E}_\Theta \langle V^2 \rangle_\beta = 2d \sum_{m=1}^M \langle h_m^2 \rangle_\beta + O(1), \quad (\text{S.32})$$

Thus, we get the bound

$$S(\rho_\beta \| \tilde{\rho}_{\beta,d}) \leq \frac{A\beta^2 M}{d} \quad (\text{S.33})$$

where $A = M^{-1} \sum_{m=1}^M h_m^2 + O(1/d)$.

Next, to derive the bounds for modes 2 and 3, we combine Lemmas 1 and 2 to express

$$\mathbb{E}_\Theta S(\rho_\beta \| \rho[\Theta]) \leq \frac{\beta^2}{2d^2} \mathbb{E}_\Theta \left(\langle V^2 \rangle_\beta - \langle V \rangle_\beta^2 \right) + \left(\frac{1}{d^3} \right). \quad (\text{S.34})$$

Similar to Eq. (S.32), we obtain

$$\mathbb{E}_\Theta \langle V \rangle_\beta^2 = 2d \sum_{m=1}^M \langle h_m \rangle_\beta^2 + O(1). \quad (\text{S.35})$$

Therefore, the expected relative entropy is

$$\mathbb{E}_\Theta S(\rho_\beta \| \rho[\Theta]) \leq \frac{C\beta^2 M}{d}, \quad (\text{S.36})$$

where we denoted

$$C = \frac{1}{M} \sum_{m=1}^M \text{Var}_\beta(h_m) + O\left(\frac{1}{d}\right) \quad (\text{S.37})$$

where $\text{Var}_\beta(x) = \langle x^2 \rangle_\beta - \langle x \rangle_\beta^2$.

By Jensen's inequality, we have

$$S(\rho_\beta \| \mathbb{E}[\rho_{\beta,d}]) \leq \mathbb{E} S(\rho_\beta \| \rho_{\beta,d}) \leq \frac{C\beta^2 M}{d} \quad (\text{S.38})$$

Using Markov's inequality, for any $x > 0$ we have

$$\text{Prob}\left(S(\rho_\beta \| \rho[\Theta]) \geq x\right) \leq \frac{1}{x} \mathbb{E}_\Theta S(\rho_\beta \| \rho[\Theta]) \quad (\text{S.39})$$

Using Eq. (S.36) and choosing $x = \mathbb{E}_\Theta S(\rho_\beta \| \rho[\Theta])/\epsilon$, we obtain the expression

$$\text{Prob}\left(S(\rho_\beta \| \rho[\Theta]) \geq \frac{C\beta^2 M}{\epsilon d}\right) \leq \epsilon. \quad (\text{S.40})$$

Thus, we prove Theorem 1.

E. Simulation of Algorithm 1

Let us first explain the simulation of noiseless circuits. Given circuit parameters Θ , as defined in Eq. (6), the outcome system-ancilla density matrix $\rho_{M,d}[\Theta] \otimes |0\rangle\langle 0|$ in system and ancilla space, where

$$\rho_{M,d}[\Theta] = \frac{1}{P_{M,d}[\Theta]} \text{Tr}_A \prod_{k=1}^d \prod_{m=1}^M \mathcal{P}_{mk} \mathcal{R}_{U_{mk}} \left(\frac{1}{2^n} I_S \otimes |0\rangle\langle 0| \right), \quad (\text{S.41})$$

where $\mathcal{R}_U(\star) = U \star U^\dagger$ is a unitary map, $U_{mk} = \exp(i\theta_{mk} h_m \otimes X_{\sigma_m})$ are unitary gates, $\mathcal{P}_{mk}(\star) = \Pi_{mk} \star \Pi_{mk}$ is the projection onto the zero state of the ancilla qubit σ_m , $\Pi_{mk} = I_{S \cup A \setminus \sigma_m} \otimes |0\rangle\langle 0|_{\sigma_m}$, and $P_{M,d}[\Theta]$ is the success probability.

The expected output state overlaps with the eigenstates of the Hamiltonian $|\mu\rangle$ is equal to

$$n_\mu = \frac{1}{N} \sum_{\Theta} P_{M,d}[\Theta] \langle \mu | \rho_{M,d}[\Theta] | \mu \rangle, \quad (\text{S.42})$$

where $|\mu\rangle$ are eigenstates of the Hamiltonian H , and the sum is formally taken over all sets of random angles and $N = \sum_{\Theta} P_{M,d}[\Theta]$ is an overall normalization factor. We estimate the expectation value using 10^3 randomly chosen angle configurations Θ . The result is shown in Fig. 2(a) (blue circled lines) for $\beta = 1$ compared to the theoretical prediction (dashed line)

$$n_\mu^{\text{theor}} = \mathcal{Z}^{-1} \exp(-\beta E_\mu), \quad \mathcal{Z} = \sum_{\mu=1}^{2^n} \exp(-\beta E_\mu). \quad (\text{S.43})$$

We also evaluate the temperature dependence of the output state energy,

$$E(\beta) = \frac{1}{N} \sum_{\Theta} P_{M,d}[\Theta] \text{Tr}(\rho_{M,d}[\Theta] H), \quad (\text{S.44})$$

and compare it to theoretical thermal value,

$$E_{\text{theor}}(\beta) = \sum_{\mu=1}^{2^n} E_\mu \exp(-\beta E_\mu). \quad (\text{S.45})$$

The output energy dependence is shown in Fig. 1(b) by blue line (circles) and the thermal value is depicted by dashed line.

Now let us consider the effects of noise. For this, we replace the output of noiseless circuit by

$$\rho_{\beta,d}^{\text{noisy}} = \frac{1}{p_{\beta,d}} \text{Tr}_A \prod_{mk} \mathcal{P}_{mk} \mathcal{R}_{U_{mk}}^{\text{noisy}} \left(\frac{1}{2^n} I_S \otimes |0\rangle\langle 0| \right), \quad (\text{S.46})$$

where, we added noise to every gate involved in the simulation as

$$R_U^{\text{noisy}} := \mathcal{D}_U \circ \mathcal{R}_U \quad (\text{S.47})$$

where

$$\mathcal{D}_U(\star) = \prod_{r \in S(U)} \left[(1 - 3p_U)(\star) + p_U \sum_{E \in S_r} E(\star) E \right] \quad (\text{S.48})$$

where $S_r = \{X_r, Y_r, Z_r\}$, $S(U)$ is support of operator U and $p_U \geq 0$ is the depolarizing error probability associated with gate U .

F. Optimized gate implementation

The representation of generic gates as standard one- and two-qubit gates is resource-demanding. There is a way to represent a generic two-qubit gate using only three two-qubit entangling gates [57]. A generic three-qubit gate, however, would require many two-qubit entangling gates to be implemented.

In our case, there is a way to avoid similar computational burdens. As we recall, ancilla qubits are measured after every gate, and we accept circuits if the measurement is zero. Therefore, each two- or three-qubit gate has a zero ancilla value in its input. Then, in the case of this particular input and Pauli terms in Eq. (15), there is a simpler method of implementing desired circuits. Gates dedicated to the terms $h_m \propto Z_i$ can be implemented, for example, by just a single entangling gate

$$\begin{aligned} R_X(\theta) |\psi\rangle |0\rangle &\equiv \\ R_X(\theta) H_i \cdot \text{CNOT}_{A \rightarrow i} \cdot H_i R_X(\theta) |\psi\rangle |0\rangle, \end{aligned} \quad (\text{S.49})$$

where H_i is Hadamard gate for qubit i , $\text{CNOT}_{A \rightarrow i}$ is a controlled NOT gate that applies to qubit i and uses the ancilla A as control, and $R_X(\theta) = \exp(\frac{1}{2} i \theta X_A)$ acts on ancilla qubit. Similarly, the gate implementing the term $h_m \propto X_i X_j$ requires only two controlled-NOT operations and single-qubit gates,

$$\begin{aligned} \exp\left(i\theta \frac{1}{2} (I + X_i X_j) X_A\right) |\psi\rangle |0\rangle &\equiv \\ R_X(\theta) \text{CNOT}_{A \rightarrow i} \text{CNOT}_{A \rightarrow j} R_X(\theta) |\psi\rangle |0\rangle, \\ \exp\left(i\theta \frac{1}{2} (I + Y_i Y_j) X_A\right) |\psi\rangle |0\rangle &\equiv \\ R_X(\theta) S_i S_j \text{CNOT}_{A \rightarrow i} \text{CNOT}_{A \rightarrow j} S_i^\dagger S_j^\dagger R_X(\theta) |\psi\rangle |0\rangle, \\ \exp\left(i\theta \frac{1}{2} (I + Z_i Z_j) X_A\right) |\psi\rangle |0\rangle &\equiv \\ R_X(\theta) H_i H_j \text{CNOT}_{A \rightarrow i} \text{CNOT}_{A \rightarrow j} H_i H_j R_X(\theta) |\psi\rangle |0\rangle, \end{aligned} \quad (\text{S.50})$$

where S_i is S -gate on i th qubit. The circuit for the Hamiltonian in Eq. (15) is shown in Fig. S1. As this circuit is built from native gates, its implementation is straightforward using tools such as IBM Qiskit.

II. DETAILS OF ALGORITHM 2

A. Proof of Theorem 2

Let us review Algorithm 2 in the main text. During thermal state preparation, the system and ancilla qubits go through multiple cycles of unitary evolution in which the ancilla must be properly reset before every cycle. In this case, the expected state of the system qubits obeys the update rule

$$\forall k \geq 0 : \quad \rho_{k+1} = \mathbb{E} \text{Tr}_A (U_k [\rho_k \otimes \sigma_k^A] U_k^\dagger), \quad (\text{S.51})$$

where $\sigma_k^A = \bigotimes_{m=1}^{n_a} [n(\omega_{mk}) |0\rangle\langle 0| + n(-\omega_{mk}) |1\rangle\langle 1|]$ is cycle-specific initial state of the ancilla, n_a is the number of ancilla qubits, $\omega_{mk} \in [-\Omega, \Omega]$ are random frequencies, $n(\omega) = (1 + \exp(\beta\omega))^{-1}$ is binary thermal distribution. The initial state of the system qubits is $\rho_0 = 2^{-n} \sum_\mu |\mu\rangle\langle \mu|$ and the unitary evolution takes the form

$$U_k = \exp(-iH^{[k]} t_k), \quad (\text{S.52})$$

where t_k are random time intervals generated from Poisson distribution $p(t) = \gamma \exp(-\gamma t)$ and H_k is given by Eq. (10) in the main text. The expectation $\mathbb{E} = \mathbb{E}_t \mathbb{E}_R \mathbb{E}_\omega$ in Eq. (S.51) is a composition of independent averages over random times t_k (\mathbb{E}_t), frequencies ω_{mk} (\mathbb{E}_ω), and the random GUE operators in $V_m^{[k]}$ (\mathbb{E}_R).

We will compare this algorithm with the Metropolis algorithm,

$$\rho_k^m = \sum_\mu \tilde{p}_{k\mu} |\mu\rangle\langle \mu|, \quad \tilde{p}_{k\mu} = \sum_\nu \Lambda_{\mu\nu}^k \tilde{p}_{k-1\nu}, \quad (\text{S.53})$$

where $\tilde{p}_{\mu k}$ are energy level occupations and transition amplitudes $\Lambda_{\mu\nu}^k = (1 - T_{\mu\nu}^k) \delta_{\mu\nu} + T_{\mu\nu}^k$. For this purpose, we use perturbation theory assuming parameters λ and γ are small and express lowest-order contribution in the dynamical equations on ρ_k in Eq. (S.52).

As a first step, it is convenient to represent the unitary map using the Liouville superoperator $\mathcal{L}_k(\star) := -i[H^{[k]}, \star]$ as

$$\exp(\mathcal{L}_k t)(\star) = U_k \star U_k^\dagger. \quad (\text{S.54})$$

Next, we use the decomposition $\mathcal{L}_k = \mathcal{L}_k^0 + \lambda \mathcal{L}_k^1$, where

$$\begin{aligned} \mathcal{L}_k^0(\star) &:= -i[H \otimes I_A + \sum_m I_S \otimes B_m^{[k]}, \star], \\ \mathcal{L}_k^1(\star) &:= -i \sum_m [I \otimes V_{q(m)}^{[k]} \otimes X_m, \star], \end{aligned} \quad (\text{S.55})$$

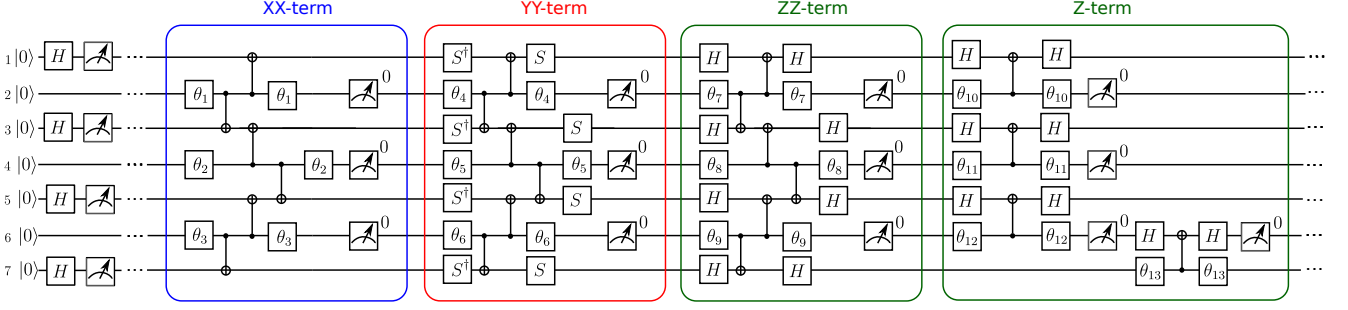


FIG. S1. **Algorithm 1 with native gates.** The circuit for Algorithm 1 contains d identical cycles; here we only show one cycle. In each cycle, three sub-cycles implement XX -terms, YY -terms, ZZ -terms, and Z -terms, according to decomposition in Eqs. (S.49) and (S.50). Gates labeled by H and S denote Hadamard gates and standard S -gates, gates labeled by θ_k (here we omitted the label of the cycle) implement unitaries $u_{km} = \exp(\frac{i}{2}\theta_k v_m X)$, $v_m = \sqrt{\beta\alpha_m/d}$, α_m is coefficient in front of Pauli term, and symbol “0” next to a box indicates postselected measurement.

and I_S, I_A are identities on the space of system and ancilla qubits respectively.

The average over time intervals can be evaluated in the superoperator representation as

$$\begin{aligned} \rho_{k+1} &= \mathbb{E}_R \mathbb{E}_\omega \mathbb{E}_t \text{Tr}_A \left[\exp(\mathcal{L}_k t) \rho_k \otimes \sigma_k^A \right] \\ &= \gamma \mathbb{E}_R \mathbb{E}_\omega \text{Tr}_A \left[\int_0^\infty dt e^{-\gamma t} \exp(\mathcal{L}_k t) \rho_k \otimes \sigma_k^A \right] \\ &= \gamma \mathbb{E}_R \mathbb{E}_\omega \text{Tr}_A \left[\frac{1}{\gamma - \mathcal{L}_k^0 - \lambda \mathcal{L}_k^1} \rho_k \otimes \sigma_k^A \right]. \end{aligned} \quad (\text{S.56})$$

The next step is to express the propagator as a series over the parameter λ (also known as Dyson’s series), resulting in the expression

$$\frac{1}{\gamma - \mathcal{L}_k^0 - \lambda \mathcal{L}_k^1} = \frac{1}{\gamma - \mathcal{L}_k^0} \sum_{\ell=0}^{\infty} \lambda^\ell \left(\mathcal{L}_k^1 \frac{1}{\gamma - \mathcal{L}_k^0} \right)^\ell. \quad (\text{S.57})$$

Our next steps are based on an ansatz. We assume the density matrix under the recursion remains diagonal up to $O(\lambda^4)$,

$$\rho_k = \sum_{\mu} p_{\mu k} |\mu\rangle\langle\mu| + O(\lambda^4), \quad (\text{S.58})$$

where $p_{\mu k} \geq 0$ are occupations of the energy levels. We will later prove that this ansatz is consistent. Upon inserting series in Eq. (S.57), we note that all contributions from odd $\ell = 2q + 1$, $q \in \mathbb{N}$, exactly vanish. This result should be expected since the ancilla is initiated on a computational basis, and superoperator \mathcal{L}_k^1 is proportional to the X operator acting on either the left or right side of the density operator. Hence, odd numbers of \mathcal{L}_k^1 always produce a zero-diagonal matrix that vanishes under partial trace transformation.

The expression in Eq. (S.56) takes the form

$$\begin{aligned} \rho_k &= \rho_{k-1} + \lambda^2 \sum_{\mu} p_{\mu k-1} C_k^{(2)}(|\mu\rangle\langle\mu|) \\ &\quad + \lambda^4 C_k^{(4)}(\rho_{k-1}) + O(\lambda^6), \end{aligned} \quad (\text{S.59})$$

where $C_k^{(\ell)}$ are linear maps defined as

$$C_k^{(\ell)}(\rho) := \gamma \mathbb{E}_{R,\omega} \text{Tr}_A \left[\frac{1}{\gamma - \mathcal{L}_k^0} \left(\mathcal{L}_k^1 \frac{1}{\gamma - \mathcal{L}_k^0} \right)^\ell \rho \otimes \sigma_k^A \right]. \quad (\text{S.60})$$

To evaluate the map for $\ell = 2$, we use

$$\begin{aligned} \mathcal{L}_k^1 |\mu\rangle\langle\nu| \otimes |a\rangle\langle b| &= -i \sum_{\alpha} V_{\alpha\mu}^{mk} |\alpha\rangle\langle\nu| \otimes |\bar{a}\rangle\langle b| \\ &\quad + i \sum_{\alpha} V_{\nu\alpha}^{mk} |\mu\rangle\langle\alpha| \otimes |a\rangle\langle\bar{b}| \end{aligned} \quad (\text{S.61})$$

where $a, b \in \{0, 1\}$, $\bar{a} = \text{NOT}(a)$, and we denoted $V_{\mu\nu}^{km} := \langle\mu|V_{q(m)}^{[k]}|\nu\rangle$. Also, we use

$$\frac{1}{\gamma - \mathcal{L}_k^0} |\mu\rangle\langle\nu| \otimes |a\rangle\langle b| = \frac{1}{\gamma - i(\Omega_{\mu\nu} + \omega_{ab})} |\mu\rangle\langle\nu| \otimes |a\rangle\langle b| \quad (\text{S.62})$$

where $\omega_{01} = \omega$, $\omega_{10} = -\omega$, and $\omega_{00} = \omega_{11} = 0$.

Then, the second order can be expressed as

$$\begin{aligned} C_k^{(2)} &= \mathbb{E}_{R,\omega} \sum_{\alpha,\nu} \sum_{s=\pm 1} n(s\omega) \left(\frac{V_{\mu\nu}^{km} V_{\alpha\mu}^{km} |\alpha\rangle\langle\nu|}{(\gamma - i(\Omega_{\mu\nu} - s\omega))(\gamma - i\Omega_{\alpha\nu})} \right. \\ &\quad \left. - \frac{V_{\mu\nu}^{km} V_{\nu\alpha}^{km} |\mu\rangle\langle\alpha|}{(\gamma - i(\Omega_{\mu\nu} + s\omega))(\gamma - i\Omega_{\mu\alpha})} + \text{h.c.} \right). \end{aligned} \quad (\text{S.63})$$

The expectation \mathbb{E}_R must be taken using ETH random-matrix ansatz in Eq. (11) in the main text,

$$\mathbb{E}_R V_{\mu\nu}^{mk} V_{\nu'\mu'}^{mk} = V_{mk}^2(E_\mu) \delta_{\mu\nu} \delta_{\mu'\nu'} + |\sigma_{\mu\nu}^{mk}|^2 \delta_{\nu\nu'} \delta_{\mu\mu'}. \quad (\text{S.64})$$

The frequency expectation \mathbb{E}_ω can be written explicitly as

$$\mathbb{E}_\omega f(\omega_{mk}) := \frac{1}{2\Omega} \int_{-\Omega}^{\Omega} d\omega f(\omega). \quad (\text{S.65})$$

Using Eqs. (S.64) and (S.65), after few algebraic transformations, we derive

$$C_k^{(2)}(|\mu\rangle\langle\mu|) = \frac{2}{\Omega} \sum_{\nu} \sum_{m=1}^M |\sigma_{\mu\nu}^{mk}|^2 \times \int_{-\Omega}^{\Omega} d\omega \frac{n(\omega)}{\gamma^2 + (\Omega_{\mu\nu} - \omega)^2} (|\nu\rangle\langle\nu| - |\mu\rangle\langle\mu|). \quad (\text{S.66})$$

Because $\Omega \geq c\|H\|$, where $c > 1$, all values $\Omega_{\mu\nu} \in [-\Omega, \Omega]$. As $\int_{-\Omega}^{\Omega} d\omega(\dots) \rightarrow \int_{-\infty}^{\infty} d\omega(\dots)(1 + O(\gamma/\Omega))$, we derive

$$\int_{-\Omega}^{\Omega} d\omega \frac{n(\omega)}{\gamma^2 + (\Omega_{\mu\nu} - \omega)^2} = \frac{\pi}{\gamma} n(\Omega_{\mu\nu}) \left(1 + O(\beta\gamma) + O\left(\frac{\gamma}{\Omega}\right)\right). \quad (\text{S.67})$$

Below we can merge the two last terms as we assume $\beta > \Omega^{-1}$ from the condition of the theorem. Inserting this expression into Eq. (S.66) and using the definition of amplitudes $T_{\mu\nu}^k$ from Eq. (13) in the main text, we get

$$C_k^{(2)}(|\mu\rangle\langle\mu|) = \sum_{\nu} T_{\mu\nu}^k (|\nu\rangle\langle\nu| - |\mu\rangle\langle\mu|) \left(1 + O(\beta\gamma)\right). \quad (\text{S.68})$$

Now we can verify the ansatz in Eq. (S.58). Indeed, all $O(\lambda^2)$ contributions are generated by the map in Eq. (S.68) that does not result in any off-diagonal elements. Then, if we start from the (diagonal) fully-mixed state, $\rho_0 = 2^{-n}I \equiv 2^{-n} \sum_{\mu} |\mu\rangle\langle\mu|$, the state remains diagonal up to $O(\lambda^2)$ order.

Now, let us consider the following CPTP map

$$\Lambda_k(\sigma) := \sum_{\nu} \Lambda_{\mu\nu}^k \sigma_{\nu\nu} |\mu\rangle\langle\mu|. \quad (\text{S.69})$$

Then, we can write the evolution for both quantum process and modeling Metropolis process in terms of this map as

$$\rho_k^m = \Lambda_k(\rho_{k-1}^m), \quad \rho_k = \Lambda_k(\rho_{k-1}) + \delta\rho_k, \quad (\text{S.70})$$

where we use the notation

$$\delta\rho_k = O(\lambda^2\beta\gamma) \sum_{\mu} T_{\mu\nu}^k p_{\mu k-1} \mathcal{D}_{\mu\nu} + \lambda^4 C_k^{(4)}(\rho_{k-1}) + O(\lambda^6) \quad (\text{S.71})$$

Using triangle inequality of the trace distance, we get

$$\begin{aligned} \delta(\rho_k|\rho_k^m) &\leq \delta(\Lambda(\rho_{k-1})|\Lambda(\rho_{k-1}^m)) + \frac{1}{2} \text{Tr} |\delta\rho_k| \\ &\leq \delta(\rho_{k-1}|\rho_{k-1}^m) + \frac{1}{2} \text{Tr} |\delta\rho_k| \end{aligned} \quad (\text{S.72})$$

By continuing this procedure, we finally get

$$\delta(\rho_d|\rho_d^m) \leq \frac{1}{2} \sum_{k=1}^d \text{Tr} |\delta\rho_k| \quad (\text{S.73})$$

From Eq. (S.71), by using triangle inequality, we get

$$\text{Tr} |\delta\rho_k| \leq O(\beta\gamma\|T^k\|) + \frac{1}{2} \text{Tr} |C_k^{(4)}(\rho_{k-1})| \quad (\text{S.74})$$

where $\|T^k\|$ is the operator norm that exhibits the asymptotic behaviour $\|T^k\| = O(n_a\lambda^2/\gamma\Omega)$.

Lemma 3 For large $1/\gamma$ and any bounded operator σ , the $\ell = 4$ map in Eq. (S.60) satisfies the asymptotic bound

$$\forall \sigma : \quad \text{Tr} |C_k^{(4)}(\sigma)| \leq O\left(\frac{n_a}{\gamma^3\Omega}\right) + O\left(\frac{n_a(n_a-1)}{\gamma^2\Omega^2}\right). \quad (\text{S.75})$$

We prove this Lemma in the following section.

Using Lemma 3, we obtain the asymptotic behaviour for the distance

$$\begin{aligned} \delta(\rho_d|\rho_d^m) &\leq O\left(d\frac{n_a\lambda^2}{\gamma\Omega}\beta\gamma\right) + O\left(d\frac{n_a\lambda^4}{\gamma^3\Omega}\right) \\ &\quad + O\left(d\frac{n_a(n_a-1)\lambda^4}{\gamma^2\Omega^2}\right) \end{aligned} \quad (\text{S.76})$$

By the statement of the theorem, we use $\Omega = c\|H\|$ as well as $d = O(D^2)$, $n_a = O(D\beta\|H\|)$, $\lambda = O(\sqrt{\epsilon}/\beta D^{3/2})$ and $\gamma = O(\epsilon/\beta D)$. Then, we get the asymptotic behavior of the first term

$$\beta d \frac{n_a\lambda^2}{\Omega} = O(\epsilon). \quad (\text{S.77})$$

In the same way, the second term scales as follows:

$$d \frac{n_a\lambda^4}{\gamma^3\Omega} = O(\epsilon). \quad (\text{S.78})$$

Finally, the third term exhibits an asymptotic behavior

$$d \frac{n_a^2\lambda^4}{\gamma^2\Omega^2} = O(\epsilon^2). \quad (\text{S.79})$$

If we combine these results, we get

$$\delta(\rho_d|\rho_d^m) \leq O(\epsilon). \quad (\text{S.80})$$

Using triangle inequality, we derive

$$\delta(\rho_d|\rho_\beta) \leq \delta(\rho_d^m|\rho_\beta) + \delta(\rho_d|\rho_d^m) \leq \delta(\rho_d^m|\rho_\beta) + O(\epsilon). \quad (\text{S.81})$$

This expression completes the proof of Theorem 2.

B. Proof of Lemma 3

The target map can be divided into four components:

$$C_k^{(4)}(\rho) = S_1(\rho) + S_2^{(1)}(\rho) + S_2^{(2)}(\rho) + S_2^{(3)}(\rho), \quad (\text{S.82})$$

where the first map describes process involving one ancilla qubit,

$$S_1(\rho) := \gamma \mathbb{E}_{R,\omega} \sum_{m=1}^{n_a} \text{Tr}_A [G_0(\mathcal{L}_{mk}^1 G_0)^4 \rho \otimes \sigma_k^A]. \quad (\text{S.83})$$

Here we denote $G_0 := (\gamma - \mathcal{L}_k^0)^{-1}$. The rest of the maps correspond to processes involving two qubits that differ in terms of their order of coupling superoperators,

$$S_2^{(1)}(\rho) := \gamma \mathbb{E}_{R,\omega} \sum_{m \neq m'}^{n_a} \text{Tr}_A [G_0(G_0 \mathcal{L}_{m'k}^1)^2 (\mathcal{L}_{mk}^1 G_0)^2 \rho \otimes \sigma_k^A], \quad (\text{S.84})$$

$$S_2^{(2)}(\rho) := \gamma \mathbb{E}_{R,\omega} \sum_{m \neq m'}^{n_a} \text{Tr}_A [G_0 \mathcal{L}_{mk}^1 G_0 (\mathcal{L}_{m'k}^1 G_0)^2 \circ \mathcal{L}_{mk}^1 G_0 \rho \otimes \sigma_k^A], \quad (\text{S.85})$$

and

$$S_2^{(3)}(\rho) := \gamma \mathbb{E}_{R,\omega} \sum_{m \neq m'}^{n_a} \text{Tr}_A [G_0(\mathcal{L}_{m'k}^1 G_0 \mathcal{L}_{mk}^1 G_0)^2 \rho \otimes \sigma_k^A]. \quad (\text{S.86})$$

We introduce the left and right components of the coupling Liouville operator, $\mathcal{L}_k^1 = \mathcal{L}_{km}^{1+} + \mathcal{L}_{km}^{1-}$, where

$$\begin{aligned} \mathcal{L}_{km}^{1+}(\sigma) &:= -i(I_C \otimes V_{q(m)}^{[k]} \otimes X_m) \cdot \sigma, \\ \mathcal{L}_{km}^{1-}(\sigma) &:= i\sigma \cdot (I_C \otimes V_{q(m)}^{[k]} \otimes X_m), \end{aligned} \quad (\text{S.87})$$

Also, we introduce $\mathcal{L}_S(\star) = -i[H \otimes I, \star]$. Then,

$$\begin{aligned} S_1(\rho) &= \mathbb{E}_\omega \sum_{s, r_i \in \pm 1} n(s\omega) \frac{1}{\gamma - \mathcal{L}_S} \mathcal{L}_{km}^{1r_4} \frac{1}{\gamma - \mathcal{L}_S - isr_3\omega} \mathcal{L}_{km}^{1r_3} \\ &\quad \times \frac{1}{\gamma - \mathcal{L}_S} \mathcal{L}_{km}^{1r_2} \frac{1}{\gamma - \mathcal{L}_S - isr_1\omega} \mathcal{L}_{km}^{1r_1} \rho. \end{aligned} \quad (\text{S.88})$$

Let us introduce $P_{\mu\nu} := |\mu\nu\rangle\langle\mu\nu|$, where $|\mu\nu\rangle$ is vector representation for the matrix element $|\mu\rangle\langle\nu|$. Then,

$$\begin{aligned} S_1(\rho) &= \sum_{m=1}^{n_a} \sum_{r_a \in \pm 1} \sum_{\mu, \nu} F_{\mu, \nu} \mathcal{P}_{\mu_4 \nu_4} \mathcal{L}_{km}^{1r_4} \mathcal{P}_{\mu_3 \nu_3} \\ &\quad \circ \mathcal{L}_{km}^{1r_3} \mathcal{P}_{\mu_2 \nu_2} \mathcal{L}_{km}^{1r_2} \mathcal{P}_{\mu_1 \nu_1} \mathcal{L}_{km}^{1r_1} \rho, \end{aligned} \quad (\text{S.89})$$

where we denoted the vectors $\boldsymbol{\mu} = \{\mu_i\}$ and $\boldsymbol{\nu} = \{\nu_i\}$, and the coefficients are

$$\begin{aligned} F_{\boldsymbol{\mu}, \boldsymbol{\nu}} &= \frac{1}{\gamma - i\Omega_{\mu_4 \nu_4}} \frac{1}{\gamma - i\Omega_{\mu_2 \nu_2}} \times \\ &\quad \times \int_{-\Omega}^{\Omega} \frac{d\omega}{\Omega} \frac{n(s\omega)}{\gamma - i(\Omega_{\mu_3 \nu_3} + sr_3\omega)(\gamma - i(\Omega_{\mu_1 \nu_1} + sr_1\omega))} \\ &\leq O\left(\frac{1}{\Omega\gamma^3}\right) \end{aligned} \quad (\text{S.90})$$

Therefore, the first map satisfies

$$\text{Tr} |S_1(\rho)| \leq O\left(\frac{n_a}{\Omega\gamma^3}\right). \quad (\text{S.91})$$

In a similar fashion, we derive

$$\begin{aligned} S_2^{(1)}(\rho) &= \sum_{m \neq m'=1}^{n_a} \sum_{r_a \in \pm 1} \sum_{\mu, \nu} B_{\mu, \nu}^1 \mathcal{P}_{\mu_4 \nu_4} \mathcal{L}_{km'}^{1r_4} \mathcal{P}_{\mu_3 \nu_3} \\ &\quad \circ \mathcal{L}_{km'}^{1r_3} \mathcal{P}_{\mu_2 \nu_2} \mathcal{L}_{km}^{1r_2} \mathcal{P}_{\mu_1 \nu_1} \mathcal{L}_{km}^{1r_1} \rho, \end{aligned} \quad (\text{S.92})$$

where the coefficient is

$$\begin{aligned} B_{\boldsymbol{\mu}, \boldsymbol{\nu}}^1 &= \sum_{s, s' \in \pm 1} \frac{1}{\gamma - i\Omega_{\mu_4 \nu_4}} \frac{1}{\gamma - i\Omega_{\mu_2 \nu_2}} \\ &\quad \times \int_{-\Omega}^{\Omega} \frac{d\omega'}{\Omega} \frac{n(s'\omega')}{\gamma - i(\Omega_{\mu_3 \nu_3} + s'r_3\omega')} \\ &\quad \times \int_{-\Omega}^{\Omega} \frac{d\omega}{\Omega} \frac{n(s\omega)}{(\gamma - i(\Omega_{\mu_1 \nu_1} + sr_1\omega))} \leq O\left(\frac{1}{\Omega^2\gamma^2}\right). \end{aligned} \quad (\text{S.93})$$

The second two-qubit process

$$\begin{aligned} S_2^{(2)}(\rho) &= \sum_{m \neq m'=1}^{n_a} \sum_{r_a \in \pm 1} \sum_{\mu, \nu} B_{\mu, \nu}^2 \mathcal{P}_{\mu_4 \nu_4} \mathcal{L}_{km}^{1r_4} \mathcal{P}_{\mu_3 \nu_3} \\ &\quad \circ \mathcal{L}_{km}^{1r_3} \mathcal{P}_{\mu_2 \nu_2} \mathcal{L}_{km'}^{1r_2} \mathcal{P}_{\mu_1 \nu_1} \mathcal{L}_{km}^{1r_1} \rho, \end{aligned} \quad (\text{S.94})$$

where the coefficient is

$$\begin{aligned} B_{\boldsymbol{\mu}, \boldsymbol{\nu}}^2 &= \sum_{s, s' \in \pm 1} \frac{1}{\gamma - i\Omega_{\mu_4 \nu_4}} \times \\ &\quad \times \int_{-\Omega}^{\Omega} \frac{d\omega}{\Omega} \frac{n(s\omega)}{[\gamma - i(\Omega_{\mu_3 \nu_3} + r_3s\omega)][\gamma - i(\Omega_{\mu_1 \nu_1} + r_1s\omega)]} \\ &\quad \times \int_{-\Omega}^{\Omega} \frac{d\omega'}{\Omega} \frac{n(s'\omega')}{\gamma - i(\Omega_{\mu_2 \nu_2} + r_2s'\omega' + r_1s\omega)} \leq O\left(\frac{1}{\Omega^2\gamma^2}\right). \end{aligned} \quad (\text{S.95})$$

Finally, the third term takes the form

$$\begin{aligned} S_2^{(3)}(\rho) &= \sum_{m \neq m'=1}^{n_a} \sum_{r_a \in \pm 1} \sum_{\mu, \nu} B_{\mu, \nu}^3 \mathcal{P}_{\mu_4 \nu_4} \mathcal{L}_{km'}^{1r_4} \mathcal{P}_{\mu_3 \nu_3} \\ &\quad \circ \mathcal{L}_{km}^{1r_3} \mathcal{P}_{\mu_2 \nu_2} \mathcal{L}_{km'}^{1r_2} \mathcal{P}_{\mu_1 \nu_1} \mathcal{L}_{km}^{1r_1} \rho \end{aligned} \quad (\text{S.96})$$

where the coefficient is

$$\begin{aligned}
B_{\mu,\nu}^3 &= \frac{1}{\gamma - i\Omega_{\mu_4\nu_4}} \int_{-\Omega}^{\Omega} \frac{d\omega}{\Omega} \frac{n(s\omega)}{\gamma - i(\Omega_{\mu_1\nu_1} + r_1 s\omega)} \\
&\times \int_{-\Omega}^{\Omega} \frac{d\omega'}{\Omega} \frac{n(s'\omega')}{\gamma - i(\Omega_{\mu_3\nu_3} + r_2 s'\omega')} \\
&\times \frac{1}{\gamma - i(\Omega_{\mu_2\nu_2} + (r_2 s'\omega' + r_1 s\omega))} \leq O\left(\frac{1}{\Omega^2 \gamma^2}\right)
\end{aligned} \tag{S.97}$$

Summarizing, we conclude that

$$\text{Tr} |S_2^{(i)}(\rho)| \leq O\left(\frac{n_a(n_a - 1)}{\Omega^2 \gamma^2}\right). \tag{S.98}$$

Using triangle inequality, we combine all the results together to establish

$$\begin{aligned}
\text{Tr} |C_k^{(4)}(\rho)| &\leq \text{Tr} |S_1(\rho)| + \sum_{i=1}^3 \text{Tr} |S_2^{(i)}(\rho)| \\
&\leq O\left(\frac{n_a}{\gamma^3 \Omega}\right) + O\left(\frac{n_a(n_a - 1)}{\gamma^2 \Omega^2}\right).
\end{aligned} \tag{S.99}$$

This concludes the proof of the Lemma.

C. Simulation of Algorithm 2

For Algorithm 2, the output of the noiseless circuit is defined as

$$\mathbb{E}[\rho_{\beta,d}] = \mathbb{E}_{\mathcal{T}} \text{Tr}_A \Psi_d \circ \dots \circ \Psi_1 \left(\frac{1}{2^n} I \right), \tag{S.100}$$

where the individual maps are

$$\Psi_k(\rho) := \text{Tr}_A \left[\mathcal{R}_{U_k}(\rho \otimes \sigma_k) \right], \tag{S.101}$$

and $\mathcal{T} = \{t_k, \omega_{mk}, a_{mk}, b_{mk}\}$ are parameters of the circuit, \mathcal{R}_{U_k} is unitary map, and U_k are defined by Eq. (S.52). For Algorithm 2, the energy level populations and the state energies are

$$n_{\mu} = \mathbb{E}_{\mathcal{T}} \langle \mu | \rho_{\beta,d} | \mu \rangle, \quad E(\beta) = \mathbb{E}_{\mathcal{T}} \text{Tr} (H \rho_{\beta,d}). \tag{S.102}$$

Similar to Algorithm 1, we simulate the noisy dynamics by adding single-qubit depolarizing channels

$$\rho_{\beta,d}^{\text{noisy}} = \text{Tr}_A \Psi_d^{\text{noisy}} \circ \dots \circ \Psi_1^{\text{noisy}} \left(\frac{1}{2^n} I \right), \tag{S.103}$$

where noisy transformation is modeled by

$$\Psi_k^{\text{noisy}}(\rho) := \text{Tr}_A \left[\mathcal{R}_{U_k}^{\text{noisy}}(\rho \otimes \sigma_k) \right] \tag{S.104}$$

Recall that the noisy unitary transformation $\mathcal{R}_{U_k}^{\text{noisy}}$ is defined in Eq. (S.48) with the error probability being $p_U = gt_k$, where g is error rate.